Multi-year high time resolution measurements of fine PM at 13 sites of the French Operational Network (CARA program): Data processing and chemical composition

Hasna Chebaicheb[1,2,3], Joel F. de Brito[1,3], Tanguy Amodeo[2,3], Florian Couvidat[2], Jean-Eudes Petit[4], Emmanuel Tison[1,3], Gregory Abbou[5], Alexia Baudic[5], Mélodie Chatain[6], Benjamin Chazeau[7,8], Nicolas Marchand[8], Raphaële Falhun[9], Florie Francony[10], Cyril Ratier[10], Didier Grenier[11], Romain Vidaud[11], Shouwen Zhang[12], Gregory Gille[13], Laurent Meunier[2,3], Caroline Marchand[2,3], Véronique Riffault[1,3], Olivier Favez[2,3]

[1]IMT Nord Europe, Institut Mines-Télécom, Université de Lille, Centre for Energy and Environment, 59000, Lille, France
[2]Institut National de l'environnement Industriel et des Risques (INERIS), 60550 Verneuil-en-Halatte, France
[3]Laboratoire Central de Surveillance de la Qualité de l'Air (LCSQA), 60550 Verneuil-en-Halatte, France
[4]Laboratoire des Sciences du Climat et de l'Environnement (LSCE), CNRS-CEA-UVSQ (UMR 8212), 91191 Gif-sur-Yvette, France
[5]Airparif, Air Quality Monitoring Network for the Greater Paris Area,75004 Paris, France
[6]Atmo Grand Est, 67300 Schiltigheim, France
[7]Laboratory of Atmospheric Chemistry, Paul Scherrer Institute, 5232 Villigen, Switzerland
[8]Aix Marseille Univ, CNRS, LCE, Marseille, France
[9]Air Breizh, 35200 Rennes, France
[10]Atmo Nouvelle-Aquitaine, 33692 Mérignac, France
[11]Atmo Auvergne Rhône-Alpes, 69500 Bron, France
[12]Atmo Hauts-de-France, 59800 Lille, France
[13]AtmoSud, Regional Network for Air Quality Monitoring of Provence-Alpes-Côte-d'Azur, Marseille, France

Correspondence to: hasna.chebaicheb@ineris.fr

Abstract. This paper presents a first comprehensive analysis of long-term measurements of atmospheric aerosol components from Aerosol Chemical Speciation Monitor (ACSM) and multi-wavelength Aethalometer (AE33) instruments collected between 2015 and 2021 at 13 (sub)urban sites as part of the French CARA program. The datasets contain the mass concentrations of major chemical species within PM_1, namely organic aerosols (OA), nitrate (NO_3^-), ammonium (NH_4^+), sulfate (SO_4^{2-}), non-sea-salt chloride (Cl^-), and equivalent black carbon (eBC). Rigorous quality control, technical validation, and environmental evaluation processes were applied, adhering to both the guidance from the French reference laboratory for air quality monitoring and the Aerosol, Clouds, and Trace gases Research Infrastructure (ACTRIS) standard operating procedures. Key findings include geographical differences in aerosol chemical composition, seasonal variations, and diel patterns, which are influenced by meteorological conditions, anthropogenic activities, and proximity to emission sources. Overall, OA dominates PM_1 at each site (43-60 % of total mass), showing distinct seasonality with higher concentrations (i) in winter, due to enhanced residential heating emissions, and (ii) in summer, due to increased photochemistry favoring secondary aerosol formation. NO_3 is the second most important contributor to PM_1 (15-30 %), peaking in late winter and early spring, especially in northern France, and playing a significant role during pollution episodes. SO_4 (8-14 %) and eBC (5-11 %) complement the major fine aerosol species, with their relative contributions strongly influenced by the origin of air masses and the stability of meteorological conditions, respectively.

A comparison with the 3D Chemical Transport Model (CTM) CHIMERE shows high correlations between simulations and measurements, albeit underestimating OA concentrations by 46-76 %. Regional discrepancies in NO_3 concentration levels emphasize the importance of these datasets in validating air quality models and tailoring air pollution mitigation strategies.

1 Introduction

The investigation of atmospheric aerosols holds significant importance in both the scientific and policy spheres due to their substantial impacts on climate (IPCC, 2021) and human health (WHO, 2021). In Europe, for instance, it is estimated that in 2021, 97 % of the urban population experienced levels surpassing the annual concentration of 5 µg m^{-3} recommended by the World Health Organization (WHO) for particulate matter with an aerodynamic diameter smaller than 2.5 µm (PM$_{2.5}$), and exposure to these fine particles was associated in 2021 with more than 253,000 premature deaths (EEA, 2023). WHO guidelines as well as regulatory thresholds set at the national level (according to the Directive 2008/50/EC for European Member States) are mainly linked with the total mass concentration of suspended particles in a given size range. However, the elaboration and evaluation of specific action plans to improve air quality require a sound knowledge of their formation, which also allows the investigation of their emission sources and chemical processes in ambient air (Viana et al., 2008, Fuzzi et al., 2015). Moreover, forecasting systems, such as those using Chemical Transport Models (CTMs), usually use chemically-speciated emission inventories as inputs, and their validation benefits from comparisons with measurements of the PM chemical composition at representative sites (e.g., Ciarelli et al., 2016, EMEP, 2022).

Historically, PM chemical speciation was mainly based on offline laboratory analyses of aerosol samples collected on filters (e.g., Putaud et al., 2004). Such methods are nowadays well standardized and provide the opportunity for comprehensive characterization of major species as well as trace compounds (EMEP, 2022). However, they are known to be subject to various sampling artifacts (Schaap et al., 2004; Wittmaack and Keck, 2004) and are collected at relatively low temporal resolution (typically 24h). They are also quite laborious and costly when used for long-term monitoring purposes. To overcome these limitations, significant efforts have been made to develop online chemical analyzers for in situ measurements in near real time. In particular, there has been a growing interest in the continuous quantification of black carbon in ambient air, especially using filter-based absorption photometers (Savadkoohi et al., 2023), given the significant influence of this aerosol component on climate (Forster et al., 2023). In parallel, the development and worldwide deployment in the last two decades of the Aerosol Mass Spectrometer (AMS, Canagaratna et al., 2007) has allowed studying non-refractory compounds (i.e., organic aerosol (OA), nitrate (NO$_3^-$), sulfate (SO$_4^{2-}$), chloride (Cl$^-$), and ammonium (NH$_4^+$)) within the fine aerosol mode (mainly PM$_1$) (Crenn et al., 2017, Lanz et al., 2010, Roig Rodelas et al., 2019, Sun et al., 2010, Zhang et al., 2017). In addition to these sophisticated high-resolution instruments, which are well suited for intensive but short-term campaigns, the Aerosol Chemical Speciation Monitor (ACSM) has been designed for continuous, multiannual measurements of the same major chemical species in the PM$_1$ or PM$_{2.5}$ fractions (Bressi et al., 2021; Chebaicheb et al., 2023; Heikkinen et al., 2021; Ng et al., 2011; Zhang et al., 2019). Both measurement methods (i.e., absorption photometers and ACSM) have become widely used in research monitoring, such as the Aerosol, Clouds, and Trace gases Research Infrastructure (ACTRIS, www.actris.eu) in Europe (Laj et al., 2024), and within the Atmospheric Science and mEasurement NeTwork (ASCENT, https://research.gatech.edu/) in the United States. Their robustness and relatively low operating costs also make them good candidates for deployment at air quality monitoring stations operated by environmental agencies (Petit et al., 2015).

In this context, since 2015, multi-wavelength Aethalometers (AE33 model, Drinovec et al., 2015) and ACSM instruments have been operated at an increasing number of urban sites in France as part of the CARA program (Chemical characterization of particulate matter, set up in 2008 by the French reference laboratory for air quality

monitoring) within the national air quality monitoring network (Favez et al., 2021), with the following main objectives: (i) to document in near real time the chemical composition (and possibly the dominant sources) of PM pollution episodes; (ii) to provide multi-year datasets of the chemical composition of the fine PM fraction, to be included into future trend analyses and/or epidemiological studies; (iii) to provide a comprehensive overview of the temporal and spatial variability of the chemical composition of fine PM over France, which can contribute in particular to evaluating and improving the accuracy of air quality models.

The main objective of this paper is to report on the chemically-speciated multi-year datasets and major findings obtained so far from these observations. After describing the quality control procedures applied to the corresponding measurements, we investigate the geographical specificities exhibited by the main chemical species within the fine PM and then provide typical seasonal and diel variations displayed by these compounds in France over the period 2015-2021. The datasets presented here are made fully available for complementary research activities, including trend analyses and epidemiological investigations. They are also vital for evaluating and validating regional air quality models through comparison exercises, examples of which are also discussed in this article using CHIMERE CTM model simulations. Indeed, the CHIMERE model is routinely validated against observations, and the online data from the CARA program play a crucial role in France for the continuous enhancement of CHIMERE, resulting in more accurate forecasts.

2 Methodology

2.1 Sites and measurement periods

The current study presents the chemical composition of fine particles within the CARA program during the period 2015-2021, at 13 sites in France, including 11 stations from regional air quality monitoring networks (AASQAs), as well as two research platforms - i.e., SIRTA (Greater Paris area) and ATOLL (Lille metropolis) - both of which are also part of the ACTRIS European research infrastructure. These stations have been gradually equipped with AE33 and ACSM instruments from 2015 onwards. A one-year (2016-2017) dataset of ACSM measurements for ATOLL (Lille), SIRTA (Paris), and Marseille Longchamp was previously integrated into a multi-site European study (Chen et al., 2022). A detailed description of the instruments is given in the next section, and the temporal coverage of the measurements considered here for each site is presented in Figure 1. A summary of each sampling site, including coordinates and related networks, can also be found in the Supplementary Information, Table S1. The majority of these sites are urban background sites, with the exception of two suburban sites (ATOLL and SIRTA) and one urban traffic site (Boulevard Périphérique Est; BPEst in Paris). Geographically distributed throughout France, these sampling sites provide a global view of the chemical composition of fine particles at the national scale.
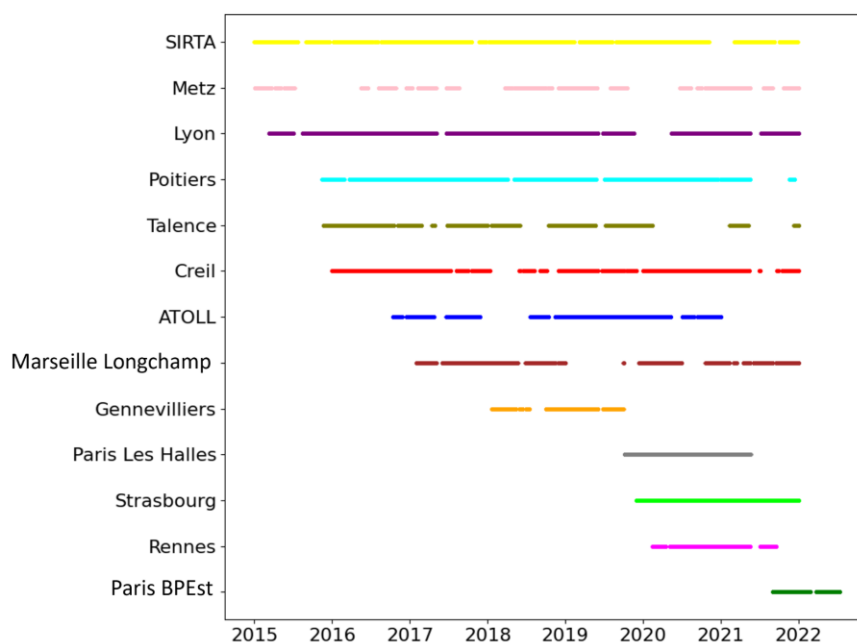
Figure 1: ACSM and AE33 measurement periods considered for each site in this study.

2.2 Non-refractory submicron aerosol measurements

2.2.1 ACSM measurement principles

The ACSM, developed by Aerodyne Research Inc., is based on mass spectrometry. As previously mentioned, it measures the chemical composition of non-refractory submicron aerosols NR-PM$_1$ in real-time, allowing long-term measurements with less monitoring and technical intervention compared to AMS, and a relatively high temporal resolution of about 30 minutes (Watson, 2017). All stations presented in this study are equipped with Quadrupole ACSMs (Q-ACSM, Ng et al., 2011), except for the Marseille-Longchamp site, where a Time-of-flight ACSM (ToF-ACSM, Fröhlich et al., 2013) is deployed. The Q-ACSM is the most commonly used analyzer because it meets the operational monitoring needs of the French monitoring agencies and is less complex than the ToF-ACSM, although the latter has lower detection limits and slightly better time resolution (about 10 minutes). More information about these instruments is presented in Table S2.

The operating principle of the ACSM is briefly described below. Ambient air first enters the vacuum system through a 100 μm diameter critical orifice. It then passes through an aerodynamic lens that focuses the aerosol into a concentrated beam, which is further directed onto a vaporizer heated at a temperature of about 600°C, causing the particles to transition to the gas phase. The gas phase molecules are then subjected to ionization at 70 eV, resulting in molecular fragmentation. The fragmented ions are guided by ion lenses to a quadrupole or time-of-flight mass filter, depending on the ACSM model.

In the ACSM, the atmospheric sample is analyzed alternatively by passing or not through a particulate filter. The air signal can thus be subtracted from the unfiltered measurements to quantify the particulate chemical species. A measurement timebase of approximately 29 min (corresponding to 28 cycles of filtered/unfiltered atmospheric samples) was used for each Q-ACSM dataset, while data were acquired with a 10 min timebase for the ToF-

143   ACSM. All ACSMs operated under the CARA program were equipped with a PM_1 aerodynamic lens and a
144   standard vaporizer.

145   In the measured mass spectra, each m/z fragment is linked to one or more species based on a fragmentation table
146   originally developed by Allan et al. (2004) and subsequently refined by Canagaratna et al. (2007). The
147   concentration of each chemical species is then obtained as the sum of its contribution in every corresponding m/z
148   fragment. Moreover, the instrument-specific response factor (RF) of NO_3 and the relative ionization efficiencies
149   (RIE) of NH_4 and SO_4 are determined by sampling 300 nm ammonium nitrate (NH_4NO_3) and ammonium sulfate
150   ((NH_4)$_2SO_4$) aerosols (Freney et al., 2019). For OA and Cl, the default RIE values of 1.4 and 1.3 are used here.
151   Finally, to obtain quantitative mass concentrations for each measured chemical species, a collection efficiency
152   (CE) correction factor is applied, following the procedure proposed by Middlebrook et al. (2011) as discussed
153   below.

154   **2.2.2 ACSM quality checks and data handling**

155   The data collected here from the ACSM instrument follows strict quality control and technical validation, including
156   an environmental evaluation involving comparison with complementary data. It has been performed following the
157   guidance provided by the French reference laboratory for air quality monitoring (LCSQA, 2018) and in full
158   agreement with the ACTRIS standard operating procedures, which are available online (https://www.actris-
159   ecac.eu/pmc-non-refractory-organics-and-inorganics.html).

160   On-site calibrations for air quality monitoring sites have been performed yearly by LCSQA personnel as well as
161   after each sensitive maintenance by the instrument distributor in Europe (ADDAIR). A detailed description of the
162   applied calibration procedures is available in a specific document edited at the national level (LCSQA, 2022).
163   Moreover, each ACSM of the CARA program has routinely participated in intercomparison exercises organized
164   by the Aerosol Chemical Monitor Calibration Centre (ACMCC) at SIRTA, to ensure proper calibration and
165   functioning of the instruments (e.g., LCSQA, 2023).

166   Given the majority of instruments used here are Q-ACSM, data processing will be detailed focusing on this model.
167   ToF-ACSM data processing (deployed at Marseille-Longchamps) is described more specifically in Chazeau et al.
168   (2021). The Q-ACSM data handling was carried out using the manufacturer's software in Igor Pro Version 6.37.
169   The first step involved checking the stability and continuity of technical parameters, including inlet pressure
170   (maintained at approximately 1.3 ± 0.2 torr), vaporizer temperature (regulated from the voltage calibration curve
171   initially defined by the manufacturer), Secondary Electron Multiplier (SEM) and Heater Bias voltages, filament
172   emission, airbeam value (set around $10^7 \pm 30\%$ ions/s), and relative humidity (ensuring it remains below 40 %
173   using a Nafion dryer upstream the inlet). Data points exhibiting inconsistencies were systematically flagged and
174   invalidated. Secondly, the calibration results, notably the RF and RIE, were carefully analyzed for consistency.
175   This approach ensured that the data cleaning process was attuned to changes in RF and RIE, thereby improving
176   the accuracy of the resulting dataset. If the RIE and RF values from two subsequent calibrations were deemed
177   comparable, their average was used. Otherwise, time-dependent RIE and RF were used, notably following
178   instrument modification. During this data cleaning phase, the CE was maintained at a constant value of 1. Thirdly,
179   data points with air (m/z 28, 32, and 40) and water (m/z 18) signal spikes were removed through a systematic
180   cleaning procedure executed within the Igor Pro software, which allows the removal of signals that appear

181 anomalous. This step also entails a comprehensive analysis of other ions to capture additional insights from the
182 data. In particular, the examination of ions associated with chloride (m/z 35 and 36) allows for checking any
183 possible measurement artifact that may be caused by sea salts (Tobler et al., 2020), while specific organic
184 compounds (m/z 43, 44, and 55), including the fragment related to levoglucosan (m/z 60), serve as a crucial
185 checkpoint for assessing the impact of distinct sources, such as biomass combustion, traffic emissions and/or
186 secondary formation processes.

187 As a next step, the implementation of the TIS (*Time series*) and RIT (*Relative Ion Transmission*) corrections were
188 performed. The TIS correction encompasses the correction of crucial time-dependent signals that exert a significant
189 influence on the measured concentrations captured by the instrument. These include the adjustment of variables
190 such as the inflow rate directed into the Q-ACSM 'reference P' (inlet pressure), the 'reference N2' signal for
191 airbeam, and the 'reference RF' for ionization efficiency. Subsequently, the RIT correction is applied to account
192 for the mass spectrometer transmission efficiency within the Q-ACSM, based on the naphthalene peaks used as
193 internal standard and represented by m/z 51, 62, 76, 102, and 128 (normalized to 1 below m/z 51 and set at 0.05
194 for m/z 154 and beyond with an exponential fit for the interval in between). We also closely examined the RIT
195 time series linked to these ions, particularly in cases where the RIT standard deviation was high. We found several
196 instances where the mean RIT value may appear satisfactory, yet the time series could have periods of anomalous
197 behavior. Thus, it is essential to carefully examine each time series of individual naphthalene masses, beyond the
198 evaluation of average RIT values alone. After these corrections, the Middlebrook algorithm (Middlebrook et al.,
199 2011), with a minimum CE of 0.5, was applied to correct the mass concentrations for the so-called composition-
200 dependent collection efficiency (CDCE) correction.

201 The following verification step involves examining the ion balance, which implies assessing the correlation
202 between the measured and predicted NH_4 concentrations, with a target slope theoretically falling within the range
203 of 1 ± 10 %, at sites and under atmospheric conditions where most aerosols should contain enough ammonium to
204 be neutral as ammonium nitrate NH_4NO_3, ammonium sulfate $(NH_4)_2SO_4$ and ammonium chloride NH_4Cl. To
205 compute the measured and predicted NH_4 concentrations, the following calculations were employed:

206 $$NH_{4,measured} = \frac{[NH_4]}{18} \tag{1}$$

207 $$NH_{4,predicted} = \frac{[NO_3]}{62} + 2\,\frac{[SO_4]}{96} + \frac{[Cl]}{35.45} \tag{2}$$

208 Finally, the analysis carefully accounted for the specific detection limits (DL) corresponding to various chemical
209 species. Following Ng et al. (2011a), DL values for Q-ACSM are 0.284, 0.148, 0.024, 0.012, and 0.011 $\mu g\ m^{-3}$
210 for NH_4, OA, SO_4, NO_3, and Cl, respectively. The same DL has been considered here for the ToF-ACSM
211 instrument deployed in Marseille-Longchamp. Data levels above the DL were validated, whereas those between -
212 $3\times DL$ and DL were replaced by DL/2. Conversely, data below $-3\times DL$ were invalidated (Table S3).

213

2.3 Equivalent Black Carbon measurements

2.3.1. Brief description of the AE33 device

Complementary to ACSM measurements, equivalent black carbon (eBC) has been monitored at all sites over the same periods using a multi-wavelength Aethalometer model AE33 (Magee Scientific). As with other filter-based absorption photometers, the AE33 primarily determines aerosol absorption coefficients (b_{abs}) at selected wavelengths, based on the rate of change in the attenuation of light transmitted through the particle-laden filter. A full description of the AE33 operating principles is given by Drinovec et al. (2015). Briefly, the instrument continuously captures aerosol particles by directing the airflow onto a specific spot on the filter tape. It assesses the aerosol by gauging the amount of light transmission that passes through a part of the filter tape containing the sample, compared to the light passing through a reference zone. In the AE33, the reference zone also samples aerosols albeit with a reduced airflow, thus at different aerosol accumulation rates, allowing for more accurate eBC and particle light absorption estimates (termed 'dual spot'). The analysis is carried out at seven optical wavelengths ranging from near-ultraviolet (UV) to near-infrared (IR) (370, 470, 525, 590, 660, 880, and 950 nm).

It should be noted that AE33 measurements used in the present paper have been performed in the PM$_1$ fraction at both ACTRIS national facilities (ATOLL and SIRTA) but in the PM$_{2.5}$ fraction at other stations. It is however considered that black carbon aerosols are overwhelmingly present in submicron particle matter (Bond et al., 2013) so that eBC concentrations discussed herewith can be (i) compared together (i.e., from one site to another), and (ii) combined with ACSM NR-PM$_1$ measurements to describe the main chemical components of fine PM at the studied sites.

2.3.2. AE33 quality checks and data handling

Similarly to ACSM measurements, the AE33 devices were operated following the LCSQA guidelines (LCSQA, 2020). The absorption coefficients used herewith were then calculated at each wavelength according to current ACTRIS guidelines (https://actris-ecac.eu/particle-light-absorption.html), following Eq. (3):

$$b_{abs} = \frac{eBC \times MAE}{H} \qquad (3)$$

where MAE represents the specific mass absorption efficiency corresponding to each wavelength (empirically determined by the manufacturer), and H is the appropriate harmonization factor to account for multiple scattering effects of the filter, which is set at 1.76 for AE33 devices using the M8060 filter tape. The eBC concentrations were then derived by normalization with a constant mass absorption cross-section (MAC$_{ACTRIS}$) recently investigated in the frame of the H2020 RI-URBANS EU research program (Alastuey et al., 2022; Savadkoohi et al., 2024), following Eq. (4):

$$eBC = \frac{b_{abs}}{MAC_{ACTRIS}} \qquad (4)$$

eBC concentrations are obtained at a wavelength of 880 nm, where it is less prone to artifacts caused by other light-absorbing compounds such as dust (notably iron oxides) and some organic compounds (termed brown carbon, BrC, which absorb light at shorter wavelengths in the UV spectrum). In ambient air, the MAC value varies from site to site and from season to season, which affects the quantification of eBC mass concentrations. The

harmonization factor was introduced by ACTRIS to standardize the calculation of absorption coefficients, depending on the filter tape used. At 880 nm, the MAC_{ACTRIS} factor used here is equivalent to 7.5 m² g^{-1}, also in good agreement with results previously obtained by Zanatta et al. (2016). It should be noted nonetheless that the application of the harmonization factor and the subsequent recalculation of eBC using a default and constant MAC value result in a reduction of about 40 % for eBC levels compared to the instrument raw outputs widely used in previous pan-European studies (such as Chen et al., 2022).

AE33 data qualification procedures include checking the AAE value obtained from the seven wavelengths for each data point, aggregated to a 15 min time base. Lower and upper acceptable AAE values of 0.7 and 3.0 are arbitrarily considered here, and the determination coefficient (r²) of the exponential fit used to calculate this AAE value must be greater than 0.9. Datapoints that did not meet these criteria were discarded. The validated data also underwent an assessment against the instrumental DL, which was set at approximately 100 ng m^{-3}. Data falling within the range of -3×DL to DL were replaced by DL/2, and data below -3×DL were invalidated (Table S3).

The source apportionment of ambient eBC concentrations is based on the model of Sandradewi et al., (2008). Briefly, the two-component model calculates the aerosol optical absorption coefficient by combining fractions associated with wood burning (wb) and fossil fuel (ff) combustion. It exploits the variations in absorption characteristics at different wavelengths. This method is based on the assumption that wood combustion has a marked absorption in the UV (high AAE) compared with fossil fuels (low AAE). For this study, and the different sites, the separation between eBC_{ff} and eBC_{wb} was performed using the values provided by the AE33 manufacturer: $AAE_{ff} = 1$ and $AAE_{wb} = 2$ (Drinovec et al., 2015).

2.4 Chemical mass closure and related uncertainties

PM_1 is a significant fraction of $PM_{2.5}$ especially in Europe (Putaud et al., 2004), understanding the composition and concentration of PM_1 is therefore essential for assessing the health risks and wider environmental impacts associated with $PM_{2.5}$ exposure. PM_1 mass was reconstructed from combining chemical species from ACSM (non-refractory $NR\text{-}PM_1 = OA + NO_3 + SO_4 + NH_4 + Cl$) and eBC from AE33 ($PM_1 = NR\text{-}PM_1 + eBC$). For each station over the study period, PM_1 mass concentrations were compared with continuous $PM_{2.5}$ measurements conducted using a tapered element oscillating microbalance equipped with the filter dynamic measurement system (TEOM-FDMS; Thermo Fisher Scientific) and/or a FIDAS 200 optical particle counter (Palas GmbH) and/or a β gauge monitor (BAM 1020; MET ONE), according to the European standard for PM regulatory measurements (EN 16450). Linear regressions of hourly data reveal fairly good agreement between the reconstructed PM_1 and the $PM_{2.5}$ mass concentrations measured at each site (Figure S1), with determination coefficients (r²) ranging from 0.72 to 0.88 (except for Marseille-Longchamp, which yielded an r² value of 0.58) and slopes varying from 0.71 to 0.99 (except for Lyon, Strasbourg, and Metz, which showed distinct lower slopes of 0.57, 0.58, and 0.61, respectively). These results confirm that $PM_{2.5}$ are predominantly made up of submicron particles and underscore the ACSM efficacy in capturing a significant proportion of that fraction at most sites. Hereafter, PM_1 (mass concentration) will be used to refer to submicron aerosol loadings estimated as the sum of eBC and $NR\text{-}PM_1$ species measured by the AE33 and ACSM, respectively.

286 Reconstructed PM_1 may overestimate measured $PM_{2.5}$ loadings mainly due to the respective measurement
287 uncertainties of each technique used here. For $PM_{2.5}$, the FIDAS instrument has been demonstrated as equivalent
288 to the EN12341 standard method with a maximum overall uncertainty of 25 % compared to this reference method
289 according to EN16450 (Amodeo, 2024). It should also be stated that this instrument is sensitive to particles above
290 180 nm optical diameter only, which may result in even higher uncertainties for the estimation of the PM_1 mass
291 fraction. For eBC, a recent intercomparison between 23 AE33 devices (Cuesta-Mosquera et al., 2021) in the
292 framework of the ACTRIS research infrastructure showed that the total mean deviation of the eBC concentrations
293 at 880 nm for the 23 instruments was -2 % (range: -16 % to 7 %) before maintenance and -1 % (range: -14 % to
294 8 %) after maintenance, for soot measurements, emphasizing that the unit-to-unit variability was not significant.
295 In our case, the post-processing of the datasets is the same for every site, therefore ensuring the comparability of
296 the obtained concentration values. However, the main uncertainty in eBC concentrations lies in the various
297 correction factors applied and not in the raw measurement itself. Considering the various approaches commonly
298 used to transform absorption coefficients into eBC mass concentrations, and related propagation of errors, an
299 overall uncertainty of up to ±50 % can be associated with eBC estimates (Savadkoohi et al., 2024). Eventually, the
300 Q-ACSM has been shown to display reproducibility uncertainties of 9 % on NR-PM_1 measurement, with
301 uncertainties of 15, 19, 28, and 36 % for NO_3, Org, SO_4, and NH_4, respectively (Crenn et al., 2015). The high
302 uncertainties of SO_4 may be related to the RIE SO_4, especially since it was considered constant in the early years.
303 Additional uncertainties are related to possible measurement artifacts associated with interferences due to the
304 nitrate (and sulfate) signal (e.g., the Pieber effect on the CO_2^+ signal at m/z 44; Pieber et al., 2016). This artifact is
305 explained by NO_3 (or SO_4)-induced reactions on the vaporizer and ionizer surfaces, producing CO_2 and therefore
306 increasing the m/z 44 signal that is otherwise attributed to the organic aerosol. It can be quantified and evaluated
307 over time by tracking the m/z 44 / NO_3 (m/z 30 / SO_4) ratios during the different calibrations performed with pure
308 ammonium nitrate (ammonium sulfate) solutions. During the ACSM intercomparison at ACMCC in 2016 (Freney
309 et al., 2019), the m/z 44 / NO_3 ratio was determined to vary between 0.01 and 0.26 for 15 instruments, and the m/z
310 30 / SO_4 ratio between 0.01 and 0.173. These were checked for each instrument in this study using calibration
311 data and the results obtained fell within these ranges thus no correction was applied. The overestimation of PM_1
312 could also be linked to a change in the chemical composition of organic aerosols when this fraction dominates
313 (e.g. Nault et al., 2023, Xu et al., 2018), since for organics the RIE is considered constant (1.4 by default) and these
314 species are not considered in the Middlebrook correction (Middlebrook et al., 2012). Finally, other uncertainties
315 can be related to size selection. It should be noted that the ACSM aerodynamic lens system is considered to be
316 fully efficient for particles from 40 nm up to 600 nm (Liu et al., 2007), while recent studies are suggesting
317 collection size ranges that might be considered as instrument-specific (Poulain et al., 2020).

318 **3 Phenomenology of fine aerosol chemistry in French urban environments**

319 **3.1 Geographical specificities in the chemical composition**

320 Figure 2 summarizes the PM_1 average values, as well as their relative contributions as pie charts and barplots,
321 calculated according to the PM_1 percentiles at various sites in France.

322   The mean PM_1 concentrations at the 13 sites range from 6.8 to 16.0 µg m^{-3}, reflecting the specificities of each

323   urban site. These levels are comparable with the annual average NR-PM_1 levels reported by Bressi et al., (2021)

324   across 21 sampling sites in Europe (from 2.8 to 14 µg m^{-3}, including remote mountain sites), with the highest NR-

325   PM_1 concentrations observed in mid-latitude Europe. In addition, Chen et al., (2022) reported an average PM_1

326   concentration of 12.2 ± 9.3 µg m^{-3} for 13 urban sites in Europe. In the present study, PM_1 averaged 9.4 ± 8.3 µg

327   m^{-3} and $PM_{2.5}$ 11.5 ± 9.2 µg m^{-3}. It is important to note that this multi-year $PM_{2.5}$ level exceeds the annual WHO

328   guideline value of 5 µg m^{-3} for $PM_{2.5}$ (WHO, 2021), as is the case at most sites in Europe (EEA, 2021).

329   Figure 3 further displays some key statistics on the various chemical species as well as for PM_1 and $PM_{2.5}$ mass

330   concentrations, as a function of mean levels measured at each site. The only site with a "Road-Traffic" typology

331   (BPEst), located on the east side of the Paris ring road, exhibits the highest mean PM_1 concentration (16.0 µg m$^-$

332   ^{3}), standing out notably on eBC, SO_4, and OA levels (Fig. 3). On the other hand, Rennes and Strasbourg display

333   the lowest mass concentrations of PM_1 (6.8 µg m^{-3}), both having the lowest levels of OA (around 3.5 µg m^{-3}). In

334   addition, the site in Rennes shows a significantly lower mean eBC level (0.4 µg m^{-3}), compared to the general

335   average (0.8 µg m^{-3}), thus depicting a lower influence of combustion aerosols at this site. The remaining sites

336   generally exhibit a fairly homogeneous PM_1 mass concentration, ranging from about 8 to 10 µg m^{-3}. ATOLL, Creil

337   and Talence sites have higher PM_1 concentrations (between 10 and 10.4 µg m^{-3}): the first two (located in the

338   northern Hauts-de-France region) are influenced by higher NO_3 concentration levels of 3.1 and 2.4 µg m^{-3},

339   respectively, whereas Talence (near Bordeaux in the southern Nouvelle-Aquitaine region) has a strong contribution

340   of OA (6.0 µg m^{-3}).

341   The high NO_3 levels at the two sites in northern France are attributed to road traffic and combustion emissions

342   (rich in nitrogen oxides; NO_x), which combine with ammonia (NH_3), typically associated with agricultural

343   activities, forming ammonium nitrate (NH_4NO_3; AN) under favorable meteorological conditions (Roig Rodelas et

344   al., 2019), as well as to transboundary pollution from Eastern Europe (Chebaicheb et al., 2023). Conversely,

345   Talence has the highest 95th percentile of OA (higher than 19.0 µg m^{-3}, Fig. 3), associated with strong biomass

346   combustion in the Bordeaux area during the cold season (Favez et al., 2021).
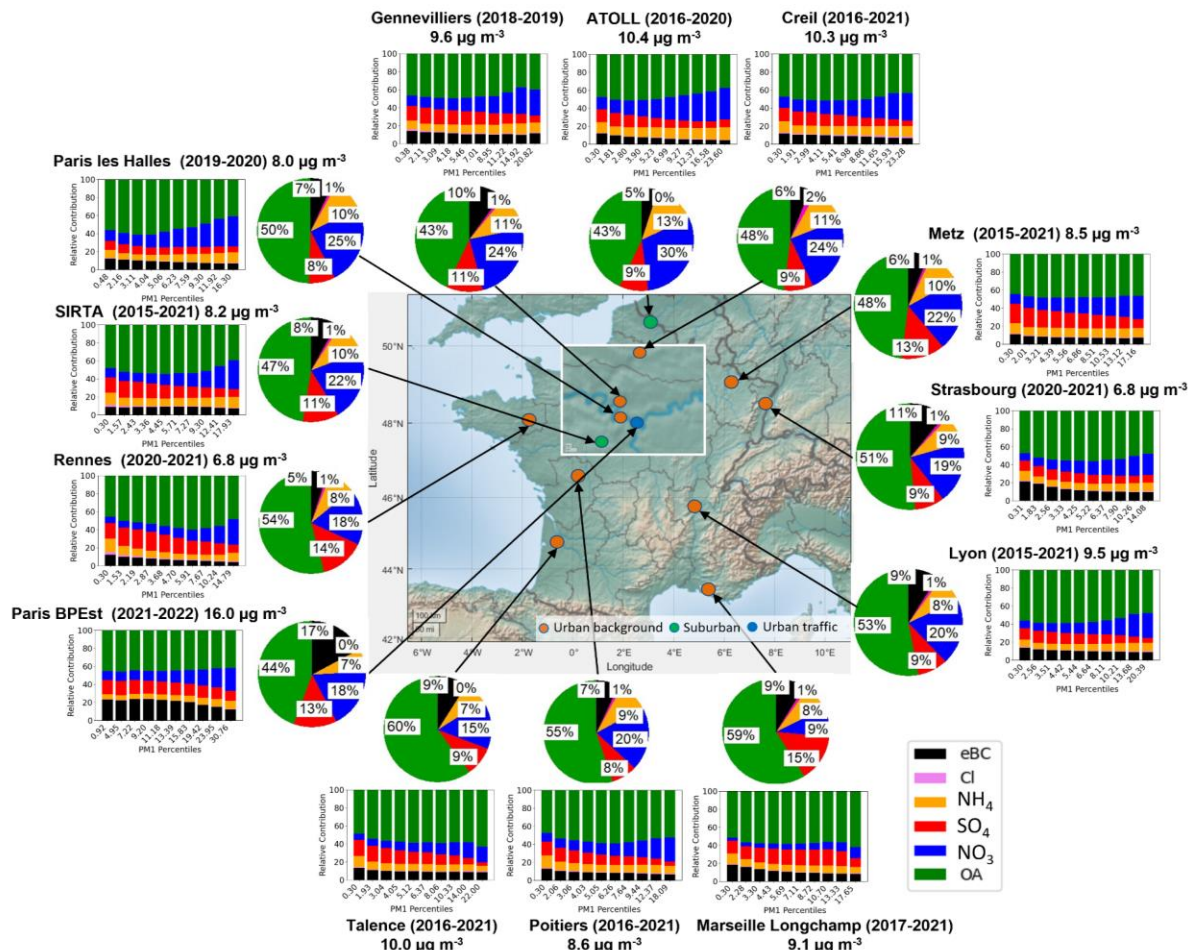
Figure 2: Multi-annual averaged PM$_1$ mass concentration and pie charts of average relative contributions of non-refractory species and eBC at different sites in France; the bar charts represent the relative contribution as a function of PM$_1$ deciles.

For the Greater Paris region, the SIRTA facility is located 22 and 25 km away from the sites representing central areas of Paris, i.e., Paris Les Halles and Gennevilliers, respectively. Logically, due to the closer proximity with intense emission sources, Gennevilliers exhibits higher PM$_1$ concentrations (9.6 µg m^{-3} on average over the 2018-2019 period) compared to SIRTA levels of 8.2 µg m^{-3}. The comparable PM$_1$ loading presented here between Paris Les Halles (8.0 µg m^{-3}) and SIRTA is probably linked to the specific measurement periods analyzed for each site. Indeed, data from Paris Les Halles presented here include the COVID-19 lockdown periods of 2020-2021, while SIRTA data are averaged over 2015-2021. When averaged over the same period as Paris Les Halles, the PM$_1$ level at SIRTA decreases to 6.2 µg m^{-3}. Moreover, an increased mixing layer height over the Paris city center, due to the urban heat island effect which may dilute the aerosol content in a wider volume during daytime, should also be considered when comparing concentrations from inner and suburban sites within such a megapolis (e.g., Dupont et al., 2016).
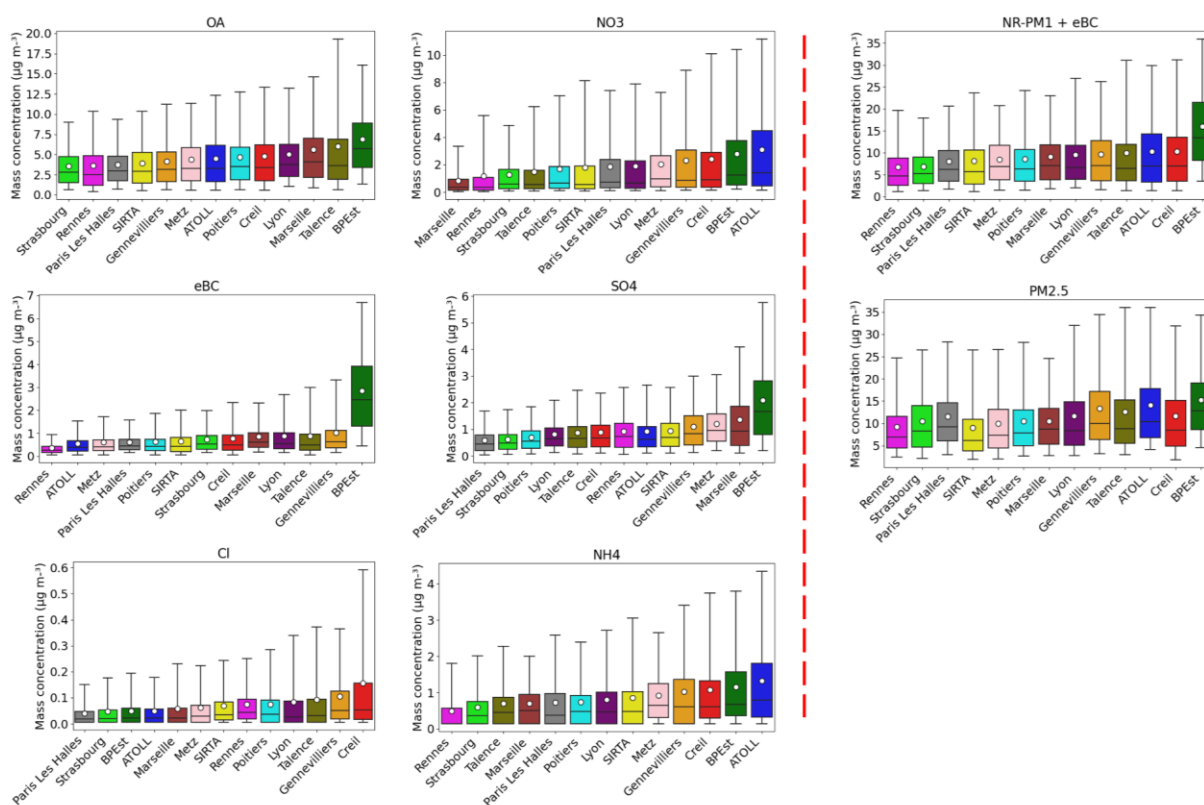
Figure 3: Box plots of the statistical distribution (5th, 25th, 50th, 75th, and 95th percentiles) of each NR-PM$_1$ species and eBC, as well as PM$_1$ and PM$_{2.5}$ mass concentrations; means are indicated by the circle symbol.

The analysis of individual contributions shows that organic compounds make up about half of the PM$_1$ total mass across all sites, ranging from 43 to 60 %, which is comparable with the average of OA at urban sites in Europe (around 50 % of PM$_1$), as reported by Chen et al., (2022). It is also consistent with the OA relative contribution observed by Bressi et al., (2021) in Europe (36-64 % of NR-PM$_1$). The stations located in central and southern France, including Marseille-Longchamp, Poitiers, Talence, and Lyon, show higher OA mass concentrations than sites in the north, which can be partly due to more intense secondary formation. Conversely, NO$_3$ contributions are more pronounced at northern sites (22-30 %, *vs* 9-20 % at southern sites), due to more favorable conditions for particulate AN formation (e.g., Favez et al., 2007). Consequently, NO$_3$ mass concentrations in France decreased from north to south and from east to west, consistent with the findings by Favez et al., (2021). Furthermore, NO$_3$ constitutes the second most significant contributor, accounting for 15-30 % of PM$_1$ mass, except for Marseille-Longchamp, where it is less than 10 % (0.8 µg m^{-3}). Other studies have also reported the predominance of NO$_3$ over SO$_4$ at many European sites (Bressi et al. 2021, Chen et al. 2022). As Marseille is characterized by high emissions from industry and shipping activities, the Marseille-Longchamp site exhibits a higher contribution of SO$_4$ (15 %), making it the second major contributor to PM$_1$ at that site (Chazeau et al., 2021).

Overall, SO$_4$ is the third largest contributor in France, with contributions ranging from 8 to 14 %. Besides Marseille-Longchamp and the BPEst traffic site, significant SO$_4$ concentrations are also obtained for Metz and Gennevilliers (around 1 µg m^{-3} on average), probably reflecting their transport from SO$_2$-rich regions, given that local emissions are considered low or negligible. Furthermore, SO$_4$ is considered to be influenced by long-range

13

385 transport from Central Europe, which is the case for many sites in northern and Eastern France, including SIRTA,
386 ATOLL, Creil, Paris Les Halles, Strasbourg, and Poitiers.

387 For the remaining compounds, mean NH_4 levels range from 0.5 to 1.3 µg m^{-3}, with a contribution fluctuating
388 between 7 % and 13 %, showing a strong correlation with NO_3 and SO_4 levels, linked to the neutralization of
389 sulfuric and nitric acids by NH_3. Meanwhile, the contribution of eBC varies from 5 to 11 % at the urban background
390 sites investigated here. Previous studies, including Chen et al. (2022), reported higher contributions of BC at
391 different European urban sites (12 %), which can be explained by recent changes in data processing, as discussed
392 in Section 2.3.2. Finally, Cl makes a minor contribution of around 1 % at all sites, with averaged mass
393 concentrations generally very low, remaining below 0.1 µg m^{-3}, except for Gennevilliers (0.1 µg m^{-3}) and Creil
394 (0.15 µg m^{-3}), with a slightly higher contribution of 2 %. Ammonium chloride (AC; NH_4Cl) is formed in the
395 atmosphere from the chemical reaction of hydrochloric acid (HCl) and NH_3. The main sources of HCl in the
396 atmosphere are biomass combustion (Andreae et al., 1996), coal burning (Tobler et al., 2020, 2021), and waste
397 combustion (McCulloch et al., 1999). In Creil, there is a large waste treatment plant 2 km northeast of the
398 monitoring station, which could explain the higher concentration of Cl observed at this site (Fig. S3). Similarly, in
399 Gennevilliers, industrial emissions could explain occasional spikes measured during easterly winds.

400 Figure 2 also illustrates the variations in PM_1 chemical composition as a function of PM_1 mass concentrations,
401 divided into 10 concentration levels (corresponding to deciles) for each site. OA exhibits even higher contributions
402 at high PM_1 mass concentrations at Talence, Marseille-Longchamp, and Poitiers especially during the coldest and
403 warmest months of the year (Figure S4). This can generally be explained by the influence of biomass burning
404 during winter pollution episodes as also previously described for the Paris area (Petit et al., 2015; Foret et al.,
405 2022), and by the impact of secondary formation of organic compounds and emissions from forest fires in summer
406 (Chen et al., 2022). However, OA decreases from the 30th percentile (around 4 to 5 µg m^{-3}) of PM_1 levels with an
407 increase in NO_3 at sites in northern France and Lyon. NO_3 plays an important role during pollution events,
408 particularly in spring, as reported previously in France (Dupont et al., 2016; Petit et al., 2017; Zhang et al., 2020)
409 and at other mid-latitude European sites (Bressi et al., 2021).

410 The contributions of SO_4 and eBC are generally stable or show a slight decrease with increasing PM_1. Nevertheless,
411 eBC exhibits significant contributions at lower PM_1 levels at BPEst and, to a lesser extent, Marseille-Longchamp,
412 Strasbourg, and Rennes, indicating significant local combustion sources at those sites. Furthermore, Marseille-
413 Longchamp exhibits fairly consistent OA, NO_3, and SO_4 contributions to PM_1 levels, showing nonetheless a
414 significant increase of the first two during pollution events. Globally, SO_4 is a relevant contributor for Metz,
415 Rennes, Gennevilliers, SIRTA, Talence, and Marseille-Longchamp, while OA retains significance at all sites
416 throughout the PM_1 percentiles.

417 **3.2 Seasonal and diel cycles of fine aerosol chemical species**

418 The averaged seasonal and diel cycles were investigated for the different chemical species at all sites. Figure 4
419 shows the median and interquartile range (IQR) monthly variability for each species considered here, over the
420 averaged cycles for the (sub)urban sites over France. The averaged monthly variabilities of the PM_1 species for
421 each site are shown in Figure S5.

All chemical species exhibit significant variability in mass concentration over the months. In particular, eBC_{wb} shows a clear seasonality, with higher concentrations during winter (around an average of 0.3 µg m^{-3}) compared to summer (0.05 µg m^{-3}), as expected due to the high level of wood combustion for residential heating in wintertime. Furthermore, there is substantial variability between sites in winter (represented by a larger IQR), probably as a result of different meteorological conditions, as well as the fraction of wood combustion for residential heating in the surroundings. Conversely, eBC_{ff} shows seasonal variations comparable to eBC_{wb}, but with smaller winter/summer difference spans ranging from around 0.4 to 0.7 µg m^{-3} in May and October, respectively. This variability is associated with seasonal meteorological conditions favoring (or not) the accumulation of atmospheric pollutants, compounded to a lesser extent to changes in road traffic intensity, leading to a maximum commonly observed in autumn (Petit et al., 2015). Similarly, OA displays higher levels during cold seasons (5.5 µg m^{-3}), with reasons comparable to those for eBC, and lower levels during warm periods (3.5 µg m^{-3}). Nevertheless, OA peaks (with a higher OA/eBC mass ratio) in summer, reflecting the formation of secondary organic aerosol (SOA) from biogenic and anthropogenic sources (Favez et al., 2007). Notably, SOAs are formed mainly from biogenic VOC in summer, when temperatures and sunlight are high (Canonaco et al., 2015; Cao et al., 2022), but also during nighttime, likely associated with nitrate chemistry (Kiendler-Scharr et al., 2016). Furthermore, OA yields lower site-to-site variability (i.e., IQR) (Fig. S6), as most of the OA, even in wintertime, is associated with regional processes and secondary formation (Chen et al., 2022; Chebaicheb et al., 2023).
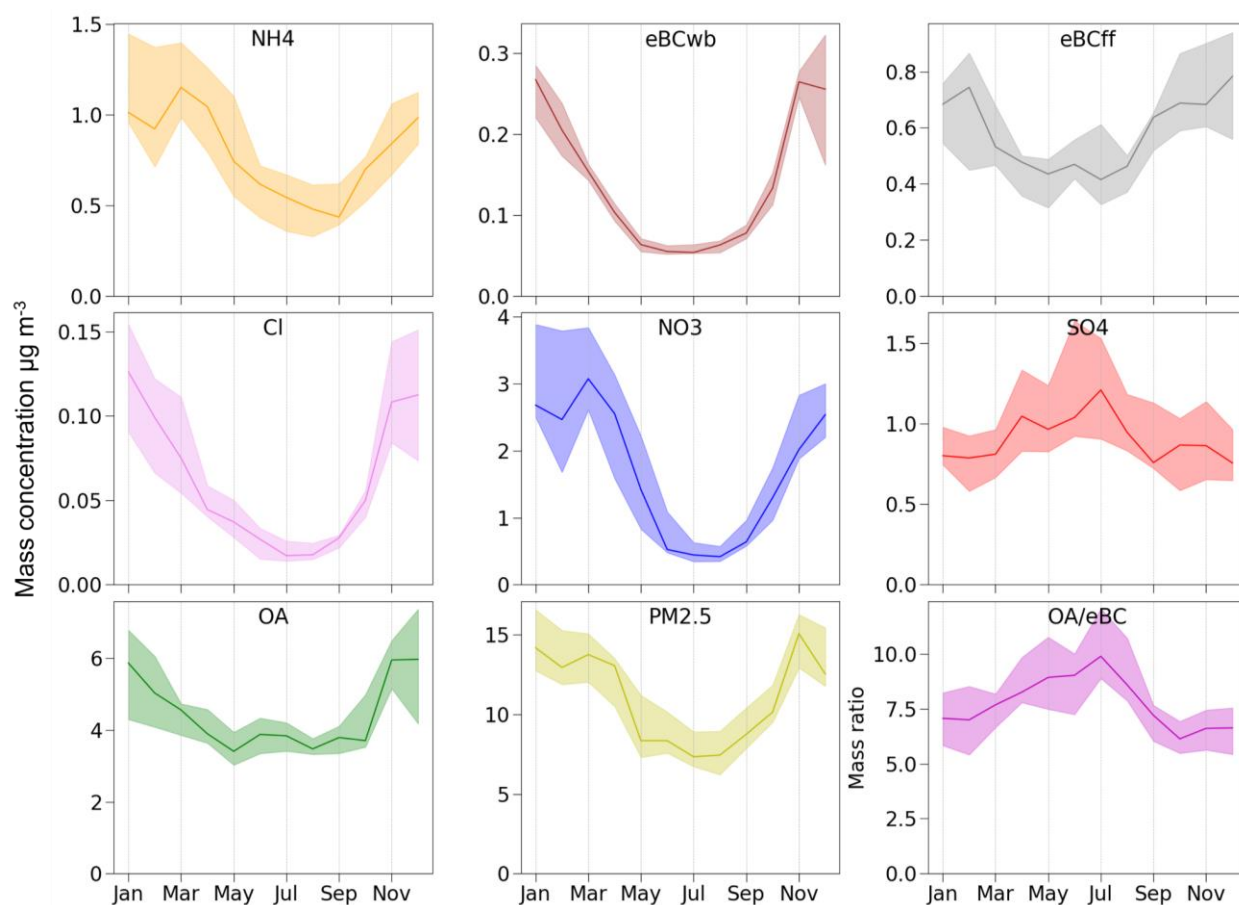

Figure 4: Monthly variability of mass concentrations of PM$_1$ species, PM$_{2.5}$, and OA/eBC ratio across all sites. The Figure shows the median and IQR (25th and 75th percentiles) calculated from the averaged monthly concentrations for each site. Months were considered only if data coverage was at least 75 %.

443

NO$_3$ and NH$_4$ concentrations display a marked seasonal pattern, peaking in late winter and early spring, and averaging around 3.0 and 1.2 µg m^{-3}, respectively. As discussed in the previous section, AN concentrations depend on site-specific factors, contributing to a greater variability between sites. In contrast, SO$_4$ shows a relatively stable monthly variation, with higher levels observed between April and August. Elevated summertime SO$_4$ concentrations could be attributed to favorable meteorological conditions. In addition, SO$_4$ can either be formed "locally" from the oxidation of SO$_2$ or transported from emission hotspots, such as Eastern European regions (Roig Rodelas et al., 2019). Cl exhibits a strong seasonality, ranging from 0.02 (summer) to 0.14 µg m^{-3} (winter). The higher concentrations of HCl during the cold seasons can be partly attributed to its semi-volatile nature (similarly to AN, its formation should be favored by low temperatures and high humidity), as well as transport from emission hotspots areas, notably of intense coal combustion, further enhanced during wintertime (Tobler et al., 2021).

The mean diel profiles obtained for each chemical species across all (sub)urban background sites and for each season are shown in Figure 5. All species exhibit higher concentrations at night, which could be, at least partially, associated with a lower boundary layer height. Some species show variability associated with local emission sources, including road traffic (morning and evening peaks), notably for OA and eBC$_{ff}$, with consistent behavior throughout the year. OA shows a stronger nighttime peak, notably during the colder months, mimicking eBC$_{wb}$ associated with wood heating. OA enhancement during nighttime in wintertime is linked with residential heating under a lower boundary layer (Favez et al., 2021). Furthermore, at Paris Les Halles, in the heart of the city center, OA further exhibits a small peak at noon (Fig. S7), pointing to a possible influence of cooking emissions at this site. Overall, the PM$_{2.5}$ profile aligns with OA diel cycles, with higher loadings during the morning and evening hours, due to the predominance of the organic species in the fine aerosol fraction.
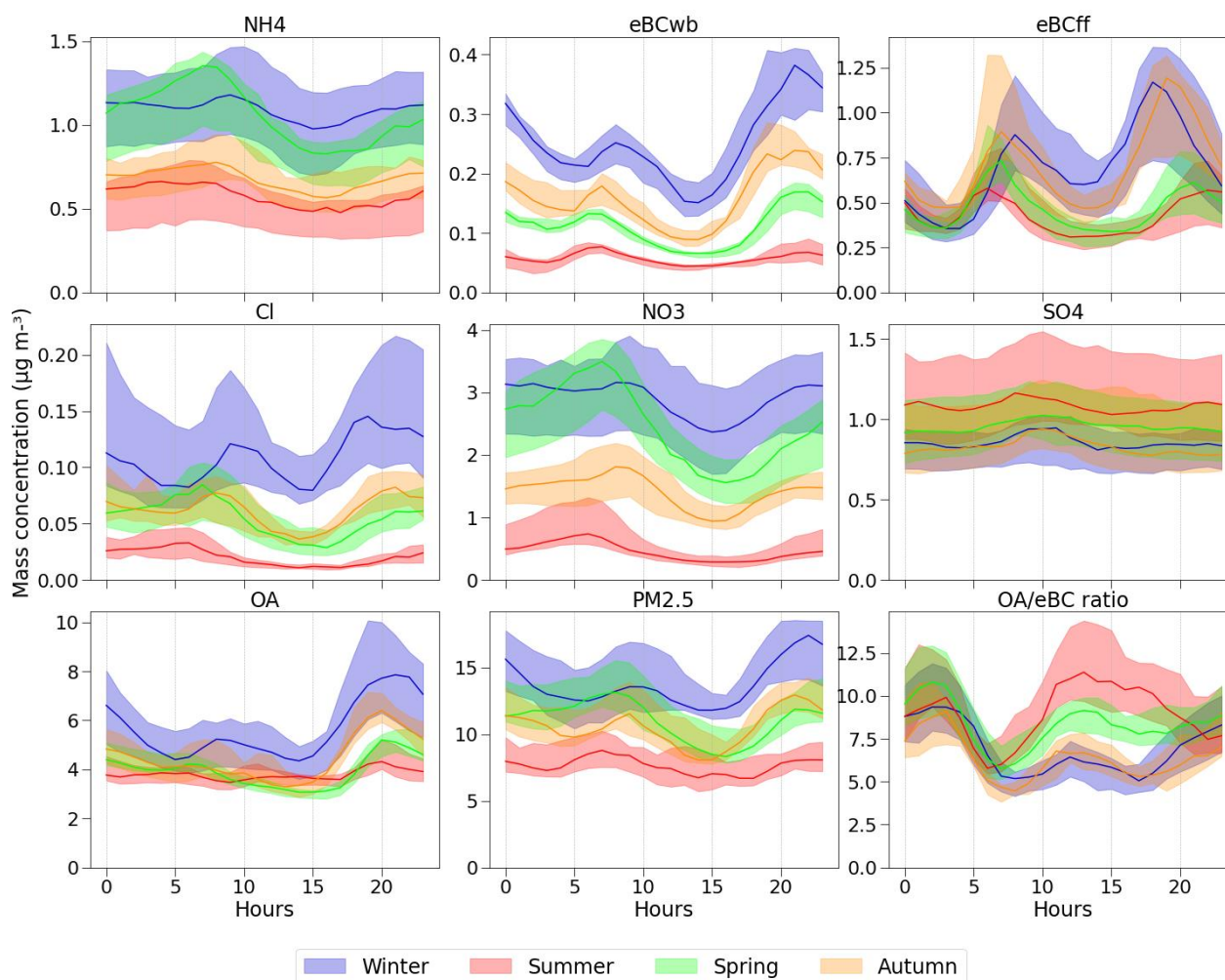
Figure 5: Seasonal median and IQR of daily profiles for all sites for each PM$_1$ component, PM$_{2.5}$, and OA/eBC ratio.

Both NO$_3$ and NH$_4$ display a comparable diel cycle, featuring higher mass concentrations during the morning hours in all seasons, albeit at different levels. Lower temperatures and higher relative humidity in the morning favor the formation of AN. During the day, as temperatures rise, AN concentrations decrease due to the evaporation into the gas phase of NH$_3$ and HNO$_3$. Consequently, AN mass concentrations are lowest in summer, due to unfavorable weather conditions and, to some extent, reduced NO$_x$ levels associated with the school holidays (Roig Rodelas et al., 2019). As discussed previously, AN levels are highest in spring, due to favorable meteorological conditions and intensive agricultural activities. On the other hand, the diel cycle of SO$_4$ shows relatively constant values during the day, with higher levels observed in summer, as discussed previously. Notably, the diel cycle of SO$_4$ at some sites features morning or afternoon peaks, especially for Lyon and Marseille-Longchamp sites, which may be explained by the presence of local (Chazeau et al., 2021) or regional sources (Fig. S7, S8, and S9).

Finally, the OA/eBC ratio shows an interesting diel cycle, exhibiting greater values at night in all seasons, ranging from 8 to 12, possibly associated with nighttime SOA formation or OA-rich sources such as wood combustion. This ratio also increases during the day, which could be explained by photochemistry and SOA formation, particularly of biogenic origin during summertime (Chebaicheb et al., 2023). As expected, the ratio decreases during the morning and evening rush hours, associated with more BC-rich traffic emissions.

17

4 Comparison between observations and the CHIMERE Chemical Transport Model

Measurements of PM chemical composition are a valuable tool for validating atmospheric CTMs, particularly for assessing their accuracy and reliability. In particular, observations and model outputs are complementary to track complex atmospheric sources and processes, including chemical transformations leading to secondary PM formation. Comparing chemically-speciated observations with CTM model results enables discrepancies to be identified and could provide clues on model improvement. In addition, near-real-time observations allow gauging a model ability to represent the temporal and spatial distributions of atmospheric pollutants, which is essential for forecasting air quality and assessing environmental policies and scenarios. The continuous observations provided by the CARA program are of great importance for the continuous improvement of 3D air quality models, notably CHIMERE, leading to more accurate forecasts and a better understanding of atmospheric processes.

4.1 Model description

In order to exemplify the comparison of our database with CTM's outputs, 3D simulations were performed with the CHIMERE version of Wang et al. (2024) which is based on a coupling between CHIMERE (Menut et al., 2021) and SSH-aerosol v1.3 aerosol model (Sartelet et al., 2020). The Secondary Organic Aerosol (SOA) mechanism of Wang et al. (2024) was used. This mechanism was obtained by using the GENOA (GENerator of reduced Organic Aerosol) v2.0 algorithm (Wang et al., 2022, 2023) to reduce the SOA mechanisms for monoterpenes and sesquiterpenes from the Master Chemical Mechanism (Saunders et al., 2003) coupled with PRAM (accounting for SOA formation from monoterpenes by auto-oxidation) (Roldin et al., 2019). Following Wang (2023), the hydrophilic/hydrophobic organics (Chrit et al., 2017) mechanism was used for other precursors. Primary organic aerosols are treated as semivolatile organic compounds that partition as a function of environmental conditions and can undergo ageing (Couvidat and Bessagnet 2021).

One important feature of SSH-aerosol consists in the computation of gas-particle partitioning with the thermodynamic module ISORROPIA (Nenes et al., 1998) and SOAP (*Secondary Organic Aerosol Processor*, Couvidat and Sartelet, 2015) models for inorganic and organic aerosols, respectively. The latter accounts for the condensation of semivolatile organic compounds onto the organic and aqueous phases of particles as well as the effect on partitioning of interactions between organic and inorganic compounds based on their molecular structure. Thermodynamic equilibrium was assumed for gas-particle partitioning.

Meteorological data were obtained from the operational analysis of the Integrated Forecasting System (IFS) model of the European Centre for Medium-Range Weather Forecasts (ECMWF) (Flentje et al., 2021). Boundary conditions were taken from CAMS CIFS (IFS coupled to a tropospheric chemistry scheme) global model simulations (Flentje et al., 2021) for chemical species. Anthropogenic emissions of gases and particles were taken from the CAMS-REG-AP inventory at a 0.05°x0.1° grid resolution (version v5.1_REF2.1) (Kuenen et al., 2022).

4.2 Comparison results

CHIMERE model results for the year 2018, with a spatial resolution of 7 km over France, were used to compare with PM_1 observations at nine of the sites where data were available (excluding BPEst, Paris Les Halles, Rennes, and Strasbourg). The time series of observed and modeled concentrations are shown in the supporting material

(Figure S10). Figure 6 summarizes results from the comparison between observations and simulations, typically showing good agreement. Loadings for inorganics (NO_3, SO_4, NH_4, and Cl) and eBC are fairly well captured by the model across all sites, with some exceptions. In particular, at the Marseille-Longchamp site, SO_4, NO_3, NH_4, and eBC are consistently underestimated by the model (33, 41, 45, and 65 %, respectively). This discrepancy could be due to the low resolution of the model grid (0.0625° x 0.125°) that may not be sufficient to capture local meteorology or sources, or more broadly a potential underestimation of emissions in the Southeastern region of France. Several sites also present an underestimation of SO_4 (Metz, SIRTA, Talence) by around 35-39 %. In contrast, NO_3 is strongly overestimated by the model (57 %) in the north of France (ATOLL). Organics, on the other hand, are consistently underestimated by the model at all sites by a factor of 2-3. Since eBC is well represented as discussed above, this leads to low modeled OA/eBC ratios (2.7-5.2, *vs* 3.9-8.8 for observed OA/eBC ratios), suggesting an underestimation of secondary organic aerosols in the model. Other recent studies also reported underestimations of OA at 11 European sites, focusing on winter 2009 (Ciarelli et al., 2016). In the present study, OA yields a strong underestimation particularly in the warmer months (60 % vs. 41 % for the colder months).
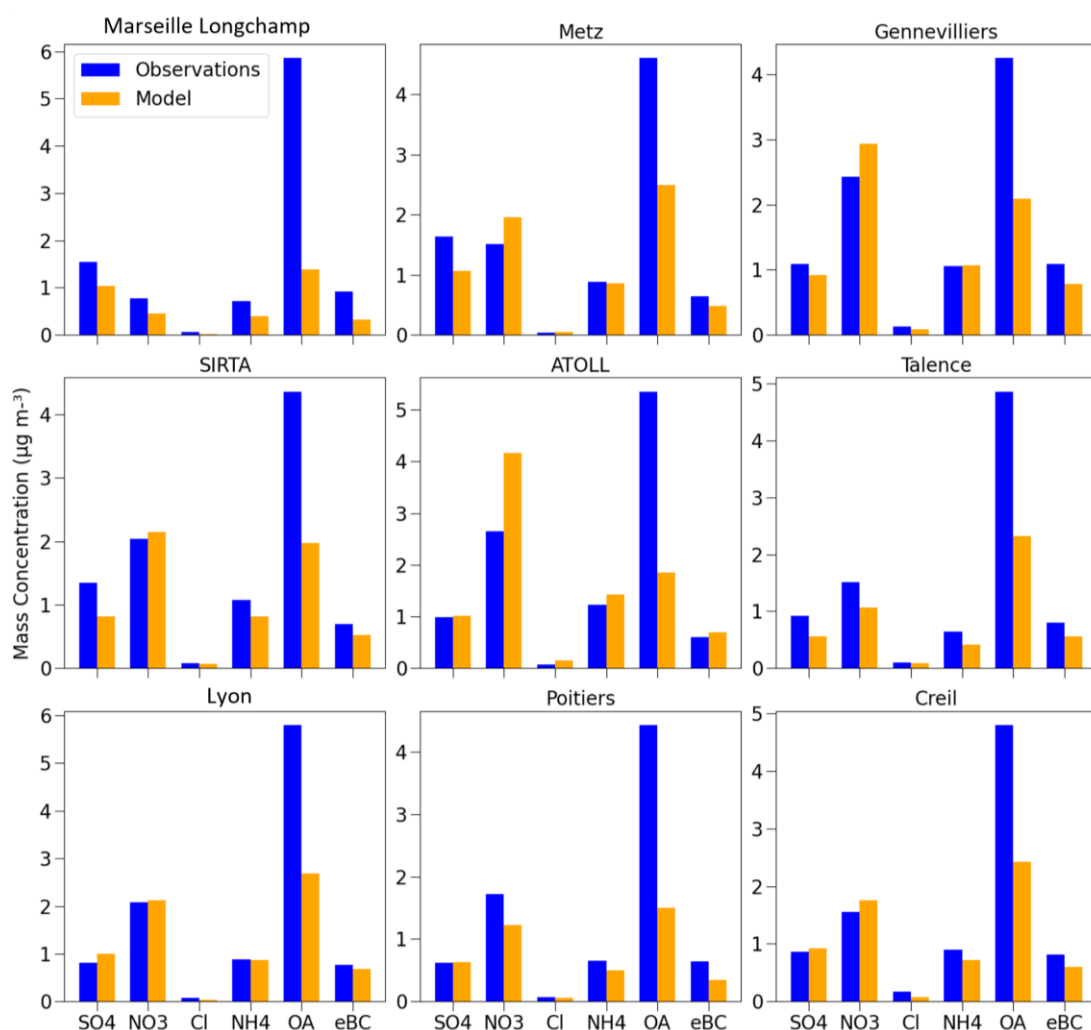

Figure 6: Mean mass concentration (in μg m^{-3}) of different chemical species for observations (in blue) and simulations (in orange) at nine French sites over the year 2018.

534 Figure 7 displays the diel profiles of each species, comparable with Figure 5, for the winter and summer of 2018
535 (spring and autumn profiles can be found in the SI, Figure S11). In general, the species exhibit relatively consistent
536 model performance between winter and summer, although there is an underestimation by the model for the latter.
537 For NO_3, the concentrations observed during wintertime are relatively stable throughout the day, whereas the
538 model shows a strong daytime decrease due to the modeled volatilization of ammonium nitrate. During
539 summertime, an enhancement of NO_3 in the early morning is captured by both observations and model, however
540 as a smooth nighttime increase/decrease for the former, and a sharp peak in the latter. A similar pattern is observed
541 for NH_4. For SO_4, the diel profile is quite constant for both observations and simulations in summer. In winter, the
542 slight increase of SO_4 during the day is not captured by the model, which instead shows a low peak at night. For
543 eBC, both observations and model simulations show two peaks during rush hours. In winter, the night peak is more
544 pronounced in the model, but nonetheless they display comparable levels, in contrast to summertime, when the
545 model tends to underestimate the concentrations. These differences in daily eBC profiles may be attributed to
546 meteorological conditions or issues in the seasonal temporality of emissions. Finally for OA, as discussed above,
547 the model largely underestimates observations in summer. Generally, the behavior is fairly well represented,
548 however the wintertime nighttime enhancement is larger than observations, similar to eBC.

549 Figure 8 presents some statistical parameters (mean bias, normalized *Root Mean Square Error* (RMSE), and
550 correlation coefficient r) calculated from the daily means for each chemical species across the nine urban sites in
551 France. Overall, the correlations between observations and model results show good agreement, with correlation
552 coefficients (r) ranging between 0.6 and 0.8, which is consistent with the literature (Couvidat et al., 2018,
553 Cholakian et al. 2018). The mean bias and normalized RMSE confirm the model robustness. Mean bias is nearly
554 negligible for SO_4, NO_3, NH_4, Cl, and eBC, and approximately -2 $\mu g\ m^{-3}$ for OA, up to -4 $\mu g\ m^{-3}$ for the Marseille
555 Longchamp site. RMSE exhibits a slightly more scattered distribution, generally ranging between 0.5 and 2 $\mu g\ m^{-3}$
556 ^{3}.

557 These comparisons between PM_1 observations and model simulations reveal underestimations or overestimations
558 by the model for each species. However, it remains challenging to pinpoint the exact reasons for these
559 discrepancies, though hypotheses can be made. Generally, there is good agreement for SO_4. On the other hand,
560 significant peaks of modeled NO_3 and NH_4 are observed, particularly in November and December at northern
561 France stations, which may be explained by an overestimation of NH_3 emissions during this period in the model
562 (Couvidat et al., 2018). For eBC, the results vary from one station to another, which may be linked to issues with
563 the spatial distribution of emissions, which are not sufficiently accurate. OA is consistently underestimated across
564 all stations. Further speciation of OA could provide more insights in this regard, which will be discussed in a
565 forthcoming article on OA sources. Ultimately, conducting further simulations over other periods could help
566 improve the model.

567

568
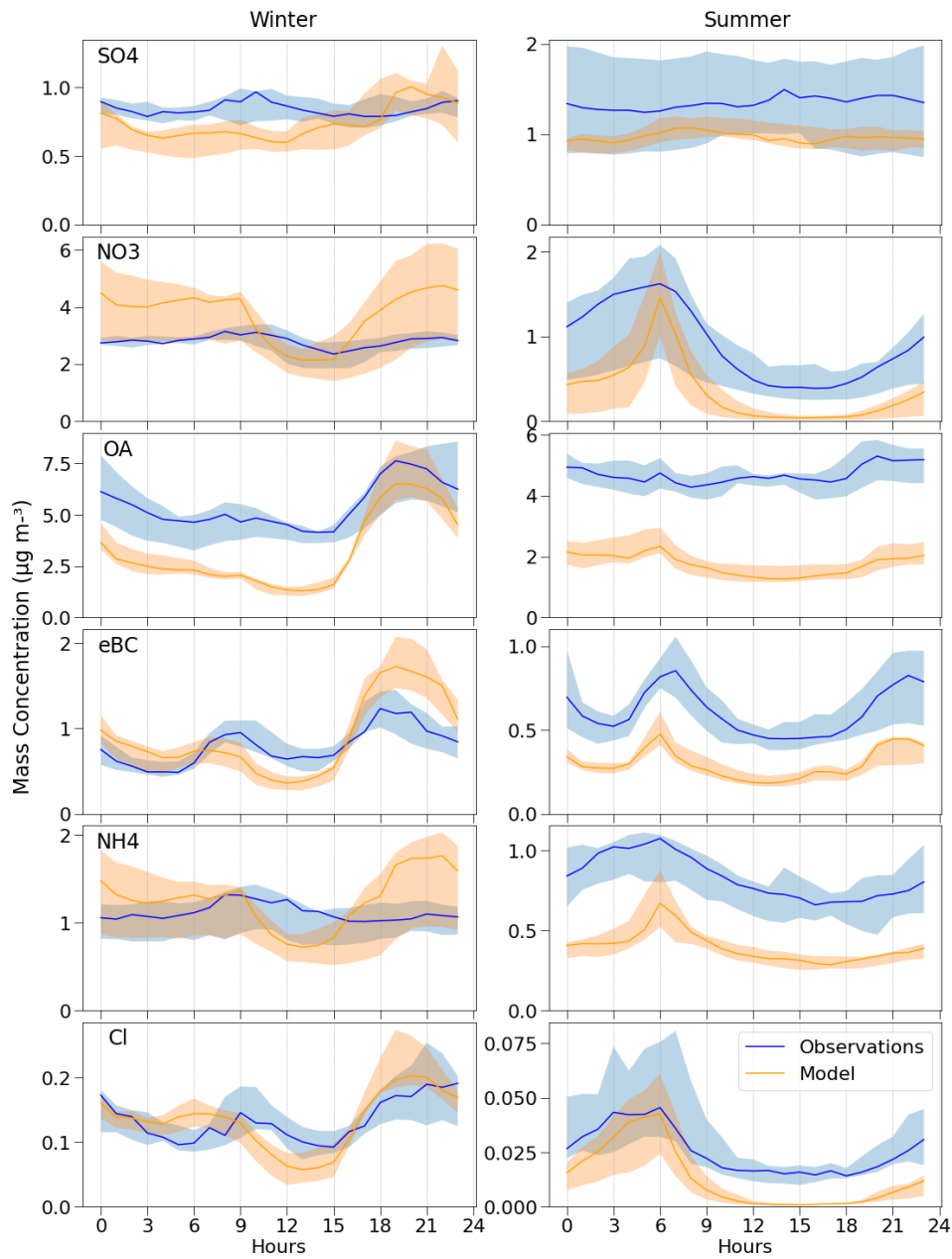
Figure 7: Observed and modeled diel profiles during the winter and summer of 2018 across 9 French sites.

569
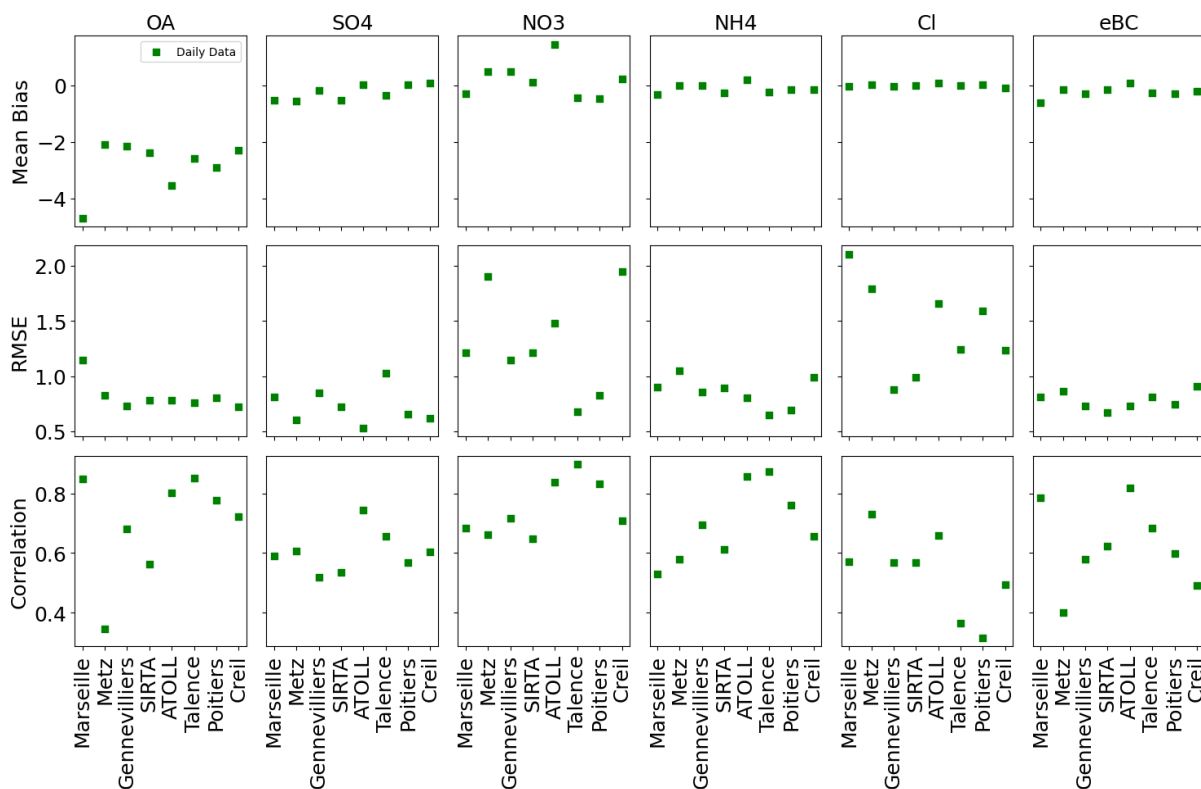
Figure 8: Statistic parameters (mean bias, normalized RMSE, and correlation coefficient r) for different species at each site, using daily averages.

Furthermore, we could compare the model results with offline chemical information from filter samples collected in the submicron aerosol fraction at four sites in 2018 within the CARA program. These filter samples were collected daily from March 15th to April 29th, 2018 in Talence, from February 16th to April 1st in Poitiers, from January 1st to January 23rd, from May 13th to May 27th, and from September 19th to September 22nd in Lyon, as well as every 4 hours from July 5th to July 27th in Marseille-Longchamp. They were analyzed in the laboratory for their organic carbon (OC), elemental carbon (EC), SO_4, NO_3, and NH_4 loadings. Figure S12 illustrates the comparison between model simulations and either online or offline observations, for these four sites with respect to OA, NO_3, NH_4, SO_4, and eBC.

A higher correlation is observed between simulations and ACSM observations for OA, NO_3, and NH_4 compared to filters (with r^2 values of 0.5, 0.7, and 0.6 with ACSM, as opposed to 0.24, 0.54, and 0.36 with filters, respectively). SO_4 and eBC show relatively similar correlations (with r^2 values of 0.44 and 0.42 with ACSM and AE33, respectively, and 0.18 and 0.11 with filters, respectively), but they exhibit different slopes (the model vs. ACSM-AE33 PM_1 demonstrates higher slopes at 0.45 and 0.5 compared to 0.36 and 0.33 with filters). Overall, the comparison of model results with observations from ACSM and AE33 shows higher correlations than with filter analyses, emphasizing the importance of online measurements for validating air quality models.

4 Conclusions

This study presents multiannual measurements of ACSM and AE33 collected at 13 (sub)urban sites that are part of the French CARA program. The datasets ranged from 1 to 6 years, between 2015 and 2021. Two of those sites

are integrated into the ACTRIS European infrastructure, namely ATOLL (near Lille) and SIRTA (near Paris). The dataset contains submicron aerosol species, OA, NO_3, NH_4, SO_4, Cl, and eBC, deconvolved into eBC_{ff} and eBC_{wb}. A meticulous process of quality control, technical validation, and environmental assessment was employed to validate homogeneously and rigorously the datasets. This process followed the guidelines provided by the French reference laboratory for air quality monitoring and adhered strictly to the ACTRIS standard operating procedures. This article presents a comprehensive overview of these long-term datasets, offering an analysis of the geographical disparities in PM_1 chemical composition, as well as the main seasonal and diel variations in fine particle content.

Across all sites, OA is the predominant compound, with a mean concentration of 4.7 µg m^{-3} (43-60 %) in PM_1, followed by NO_3 (15-30 %), SO_4 (8-14 %), NH_4 (7-13 %), and eBC (5-11 %). Stations in central and southern France exhibit higher OA mass concentrations (5.3 µg m^{-3}), likely attributed to more pronounced photochemical formation processes. Such secondary processes may also explain that OA is the predominant compound for the highest concentration levels in summertime at all sites (Figure S4). Additionally, for other seasons, OA exhibits greater contributions (>55 %) during periods of elevated PM_1 levels in the southern half of France, while NO_3 contributions (>40 %) are more notable during pollution episodes at northern sites, illustrating the competing influences on the aerosol chemical composition of biomass burning emissions and favorable meteorological conditions leading to the formation of ammonium nitrate, depending on the site location.

Temporal variations reveal distinct seasonality in PM_1 chemical species. eBC_{wb} and OA peak during wintertime, with values of around 0.3 and 5.5 µg m^{-3}, respectively, typically associated with increased residential heating emissions. Those values peak particularly at night, combining stronger emissions and a potentially shallower boundary layer height, facilitating pollutant accumulation. OA also peaks in summer (3.5 µg m^{-3}), typically associated with enhanced SOA formation. NO_3 peaks in late winter and early spring, correlated with a typical increase of NH_3 and favorable meteorological conditions during cold periods. Diel variations also exhibit unique characteristics at certain sites, such as the Paris Les Halles site, where an organic peak at noon suggests a significant contribution from cooking activities; similarly, a more pronounced rush hour enhancement at BPEst suggests a strong role of local traffic on OA levels.

Furthermore, the datasets presented here serve as essential tools for evaluating and validating regional and global air quality models. An illustrative comparison with CHIMERE is presented in this paper for 2018, encompassing nine French sites. Generally, the model successfully simulates inorganics (NO_3, SO_4, NH_4) and eBC but underestimates OA by 46-76 %, although with a high correlation between simulations and measurements (r between 0.6 and 0.8). Notably, NO_3 seems to be overestimated at the ATOLL site in northern France (57 %), whereas it is substantially underestimated by 29-42 % at southern sites. Overall, these multi-year datasets from French urban background sites hold significant value for the scientific community, enabling future research endeavors, including source apportionment studies, trend analyses, and epidemiological and health-related investigations.

Author contributions

Data curation & Formal analysis	Mélodie Chatain, Benjamin Chazeau, Hasna Chebaicheb, Jean-Eudes Petit, Shouwen Zhang
Funding acquisition	Olivier Favez, Véronique Riffault
Investigation	Hasna Chebaicheb
Methodology	Hasna Chebaicheb
Resources	Gregory Abbou, Alexia Baudic, Mélodie Chatain, Benjamin Chazeau, Florian Couvidat, Raphaële Falhun, Florie Francony, Gregory Gille, Didier Grenier, Nicolas Marchand, Jean-Eudes Petit, Cyril Ratier, Véronique Riffault, Romain Vidaud, Shouwen Zhang
Supervision	Joel F. de Brito, Olivier Favez, Caroline Marchand, Véronique Riffault
Validation	Joel F. de Brito, Olivier Favez, Caroline Marchand, Véronique Riffault
Visualization	Hasna Chebaicheb
Writing – original draft preparation	Hasna Chebaicheb, Olivier Favez
Writing – review & editing	All co-authors

645   **Conflicts of Interest.** The authors declare no conflict of interest.

646   **References**

647   Allan, J. D., Delia, A. E., Coe, H., Bower, K. N., Alfarra, M. R., Jimenez, J. L., Middlebrook, A. M., Drewnick,

648   F., Onasch, T. B., Canagaratna, M. R., Jayne, J. T., and Worsnop, D. R.: A generalised method for the extraction

649   of chemically resolved mass spectra from Aerodyne aerosol mass spectrometer data, J. Aerosol Sci., 35, 909–922,

650   https://doi.org/10.1016/j.jaerosci.2004.02.007, 2004.

651   Alastuey, A., Querol, X., García, M., Trechera, P., Savadkoohi, M., Karanasiou, A., Minguillón, M. C., Fiebig,

652   M., Dallënbach, K. R., Salameh, T., Sauvage, S., and Petäjä, T.: Deliverable D1 (D1.1): Guidelines, datasets of

653   non-regulated pollutants incl. metadata, methods, 2022.

654   Amodeo, T., 2024. Guide méthodologique pour la surveillance des PM10 et PM2.5 dans l'air ambiant par méthode

655   optique FIDAS (révision 2023) | LCSQA. https://www.lcsqa.org/fr/rapport/guide-methodologique-pour-la-

656   surveillance-des-pm10-et-pm25-dans-lair-ambiant-par-methode-0 (accessed 8.13.24).

657   Bond, T. C., Doherty, S. J., Fahey, D. W., Forster, P. M., Berntsen, T., DeAngelo, B. J., Flanner, M. G., Ghan, S.,

658   Kärcher, B., Koch, D., Kinne, S., Kondo, Y., Quinn, P. K., Sarofim, M. C., Schultz, M. G., Schulz, M.,

659   Venkataraman, C., Zhang, H., Zhang, S., Bellouin, N., Guttikunda, S. K., Hopke, P. K., Jacobson, M. Z., Kaiser,

660   J. W., Klimont, Z., Lohmann, U., Schwarz, J. P., Shindell, D., Storelvmo, T., Warren, S. G., and Zender, C. S.:

661   Bounding the role of black carbon in the climate system: A scientific assessment, J. Geophys. Res. Atmospheres,

662   118, 5380–5552, https://doi.org/10.1002/jgrd.50171, 2013.

663   Bressi, M., Cavalli, F., Putaud, J. P., Fröhlich, R., Petit, J.-E., Aas, W., Äijälä, M., Alastuey, A., Allan, J. D.,

664   Aurela, M., Berico, M., Bougiatioti, A., Bukowiecki, N., Canonaco, F., Crenn, V., Dusanter, S., Ehn, M., Elsasser,

665   M., Flentje, H., Graf, P., Green, D. C., Heikkinen, L., Hermann, H., Holzinger, R., Hueglin, C., Keernik, H.,

666   Kiendler-Scharr, A., Kubelová, L., Lunder, C., Maasikmets, M., Makeš, O., Malaguti, A., Mihalopoulos, N.,

667   Nicolas, J. B., O'Dowd, C., Ovadnevaite, J., Petralia, E., Poulain, L., Priestman, M., Riffault, V., Ripoll, A.,

668   Schlag, P., Schwarz, J., Sciare, J., Slowik, J., Sosedova, Y., Stavroulas, I., Teinemaa, E., Via, M., Vodička, P.,

669   Williams, P. I., Wiedensohler, A., Young, D. E., Zhang, S., Favez, O., Minguillón, M. C., and Prevot, A. S. H.: A

670   European aerosol phenomenology - 7: High-time resolution chemical characteristics of submicron particulate

671   matter across Europe, Atmospheric Environ. X, 10, 100108, https://doi.org/10.1016/j.aeaoa.2021.100108, 2021.

672   Canagaratna, M. r., Jayne, J. t., Jimenez, J. l., Allan, J. d., Alfarra, M. r., Zhang, Q., Onasch, T. b., Drewnick, F.,

673   Coe, H., Middlebrook, A., Delia, A., Williams, L. r., Trimborn, A. m., Northway, M. j., DeCarlo, P. f., Kolb, C.

674   e., Davidovits, P., and Worsnop, D. r.: Chemical and microphysical characterization of ambient aerosols with the

675   aerodyne aerosol mass spectrometer, Mass Spectrom. Rev., 26, 185–222, https://doi.org/10.1002/mas.20115,

676   2007.

677   Canonaco, F., Slowik, J. G., Baltensperger, U., and Prévôt, A. S. H.: Seasonal differences in oxygenated organic

678   aerosol composition: implications for emissions sources and factor analysis, Atmospheric Chem. Phys., 15, 6993–

679   7002, https://doi.org/10.5194/acp-15-6993-2015, 2015.

Chazeau, B., Temime-Roussel, B., Gille, G., Mesbah, B., D'Anna, B., Wortham, H., and Marchand, N.: Measurement report: Fourteen months of real-time characterisation of the submicronic aerosol and its atmospheric dynamics at the Marseille–Longchamp supersite, Atmospheric Chem. Phys., 21, 7293–7319, https://doi.org/10.5194/acp-21-7293-2021, 2021.

Chazeau, B., El Haddad, I., Canonaco, F., Temime-Roussel, B., D'Anna, B., Gille, G., Mesbah, B., Prévôt, A.S.H., Wortham, H., Marchand, N., 2022. Organic aerosol source apportionment by using rolling positive matrix factorization: Application to a Mediterranean coastal city. Atmospheric Environment: X 14, 100176. https://doi.org/10.1016/j.aeaoa.2022.100176

Chebaicheb, H., F. de Brito, J., Chen, G., Tison, E., Marchand, C., Prévôt, A. S. H., Favez, O., and Riffault, V.: Investigation of four-year chemical composition and organic aerosol sources of submicron particles at the ATOLL site in northern France, Environ. Pollut., 330, 121805, https://doi.org/10.1016/j.envpol.2023.121805, 2023.

Chebaicheb, H., Ferreira De Brito, J., Amodeo, T., Couvidat, F., Petit, J.-E., Tison, E., Abbou, G., Alexia, B., Chatain, M., Chazeau, B., Marchand, N., Falhun, R., Francony, F., Ratier, C., Grenier, D., Vidaud, R., Zhang, S., Gille, G., Meunier, L., Marchand, C., Riffault, V., and Favez, O.: Multi-year high time resolution measurements of fine PM at 13 sites of the French Operational Network (CARA program), https://doi.org/10.5281/zenodo.13318298.

Chen, G., Canonaco, F., Tobler, A., Aas, W., Alastuey, A., Allan, J., Atabakhsh, S., Aurela, M., Baltensperger, U., Bougiatioti, A., De Brito, J. F., Ceburnis, D., Chazeau, B., Chebaicheb, H., Daellenbach, K. R., Ehn, M., El Haddad, I., Eleftheriadis, K., Favez, O., Flentje, H., Font, A., Fossum, K., Freney, E., Gini, M., Green, D. C., Heikkinen, L., Herrmann, H., Kalogridis, A.-C., Keernik, H., Lhotka, R., Lin, C., Lunder, C., Maasikmets, M., Manousakas, M. I., Marchand, N., Marin, C., Marmureanu, L., Mihalopoulos, N., Močnik, G., Nęcki, J., O'Dowd, C., Ovadnevaite, J., Peter, T., Petit, J.-E., Pikridas, M., Matthew Platt, S., Pokorná, P., Poulain, L., Priestman, M., Riffault, V., Rinaldi, M., Różański, K., Schwarz, J., Sciare, J., Simon, L., Skiba, A., Slowik, J. G., Sosedova, Y., Stavroulas, I., Styszko, K., Teinemaa, E., Timonen, H., Tremper, A., Vasilescu, J., Via, M., Vodička, P., Wiedensohler, A., Zografou, O., Cruz Minguillón, M., and Prévôt, A. S. H.: European aerosol phenomenology − 8: Harmonised source apportionment of organic aerosol using 22 Year-long ACSM/AMS datasets, Environ. Int., 166, 107325, https://doi.org/10.1016/j.envint.2022.107325, 2022.

Campagne 2021 d'étalonnage et de comparaison inter-laboratoire (CIL) des Q-ACSM | LCSQA: https://www.lcsqa.org/fr/rapport/campagne-2021-detalonnage-et-de-comparaison-inter-laboratoire-cil-des-q-acsm, last access: 24 October 2023.

Cholakian, A., Beekmann, M., Colette, A., Coll, I., Siour, G., Sciare, J., Marchand, N., Couvidat, F., Pey, J., Gros, V., Sauvage, S., Michoud, V., Sellegri, K., Colomb, A., Sartelet, K., Langley DeWitt, H., Elser, M., Prévot, A. S. H., Szidat, S., and Dulac, F.: Simulation of fine organic aerosols in the western Mediterranean area during the ChArMEx 2013 summer campaign, Atmospheric Chem. Phys., 18, 7287–7312, https://doi.org/10.5194/acp-18-7287-2018, 2018.

Chrit, M., Sartelet, K., Sciare, J., Pey, J., Marchand, N., Couvidat, F., Sellegri, K., and Beekmann, M.: Modelling organic aerosol concentrations and properties during ChArMEx summer campaigns of 2012 and 2013 in the western Mediterranean region, Atmospheric Chem. Phys., 17, 12509–12531, https://doi.org/10.5194/acp-17-12509-2017, 2017.

Ciarelli, G., Aksoyoglu, S., Crippa, M., Jimenez, J.-L., Nemitz, E., Sellegri, K., Äijälä, M., Carbone, S., Mohr, C., O'Dowd, C., Poulain, L., Baltensperger, U., and Prévôt, A. S. H.: Evaluation of European air quality modelled by CAMx including the volatility basis set scheme, Atmospheric Chem. Phys., 16, 10313–10332, https://doi.org/10.5194/acp-16-10313-2016, 2016.

Couvidat, F. and Sartelet, K.: The Secondary Organic Aerosol Processor (SOAP v1.0) model: a unified model with different ranges of complexity based on the molecular surrogate approach, Geosci. Model Dev., 8, 1111–1138, https://doi.org/10.5194/gmd-8-1111-2015, 2015.

Couvidat, Florian, and Bertrand Bessagnet. 2021. « Role of ecosystem-atmosphere exchanges of semi-volatile organic compounds in organic aerosol formation ». Atmospheric Environment 263 (octobre): 118541. https://doi.org/10.1016/j.atmosenv.2021.118541.

Couvidat, Florian, Bertrand Bessagnet, Marta Garcia-Vivanco, Elsa Real, Laurent Menut, et Augustin Colette. 2018. « Development of an Inorganic and Organic Aerosol Model (CHIMERE 2017β v1.0): Seasonal and Spatial Evaluation over Europe ». Geoscientific Model Development 11 (1): 165-94. https://doi.org/10.5194/gmd-11-165-2018.

Crenn, V., Sciare, J., Croteau, P.L., Verlhac, S., Fröhlich, R., Belis, C.A., Aas, W., Äijälä, M., Alastuey, A., Artiñano, B., Baisnée, D., Bonnaire, N., Bressi, M., Canagaratna, M., Canonaco, F., Carbone, C., Cavalli, F., Coz, E., Cubison, M.J., Esser-Gietl, J.K., Green, D.C., Gros, V., Heikkinen, L., Herrmann, H., Lunder, C., Minguillón, M.C., Močnik, G., O'Dowd, C.D., Ovadnevaite, J., Petit, J.-E., Petralia, E., Poulain, L., Priestman, M., Riffault, V., Ripoll, A., Sarda-Estève, R., Slowik, J.G., Setyan, A., Wiedensohler, A., Baltensperger, U., Prévôt, A.S.H., Jayne, J.T., Favez, O., 2015. ACTRIS ACSM intercomparison – Part 1: Reproducibility of concentration and fragment results from 13 individual Quadrupole Aerosol Chemical Speciation Monitors (Q-ACSM) and consistency with co-located instruments. Atmospheric Measurement Techniques 8, 5063–5087. https://doi.org/10.5194/amt-8-5063-2015.

Crenn, V., Fronval, I., Petitprez, D., Riffault, V., 2017. Fine particles sampled at an urban background site and an industrialized coastal site in Northern France — Part 1: Seasonal variations and chemical characterization. Sci. Total Environ. 578, 203–218. https://doi.org/10.1016/j.scitotenv.2015.11.165.

Cuesta-Mosquera, A., Močnik, G., Drinovec, L., Müller, T., Pfeifer, S., Minguillón, M.C., Briel, B., Buckley, P., Dudoitis, V., Fernández-García, J., Fernández-Amado, M., Ferreira De Brito, J., Riffault, V., Flentje, H., Heffernan, E., Kalivitis, N., Kalogridis, A.-C., Keernik, H., Marmureanu, L., Luoma, K., Marinoni, A., Pikridas, M., Schauer, G., Serfozo, N., Servomaa, H., Titos, G., Yus-Díez, J., Zioła, N., Wiedensohler, A., 2021. Intercomparison and characterization of 23 Aethalometers under laboratory and ambient air conditions: procedures

750 and unit-to-unit variabilities. Atmospheric Measurement Techniques 14, 3195–3216. https://doi.org/10.5194/amt-
751 14-3195-2021.

752 Daellenbach, K. R., Bozzetti, C., Křepelová, A., Canonaco, F., Wolf, R., Zotter, P., Fermo, P., Crippa, M., Slowik,
753 J. G., Sosedova, Y., Zhang, Y., Huang, R.-J., Poulain, L., Szidat, S., Baltensperger, U., El Haddad, I., and Prévôt,
754 A. S. H.: Characterization and source apportionment of organic aerosol using offline aerosol mass spectrometry,
755 Atmospheric Meas. Tech., 9, 23–39, https://doi.org/10.5194/amt-9-23-2016, 2016.

756 Drinovec, L., Močnik, G., Zotter, P., Prévôt, A. S. H., Ruckstuhl, C., Coz, E., Rupakheti, M., Sciare, J., Müller,
757 T., Wiedensohler, A., and Hansen, A. D. A.: The "dual-spot" Aethalometer: an improved measurement of aerosol
758 black carbon with real-time loading compensation, Atmospheric Meas. Tech., 8, 1965–1979,
759 https://doi.org/10.5194/amt-8-1965-2015, 2015.

760 Dupont, J.-C., Haeffelin, M., Badosa, J., Elias, T., Favez, O., Petit, J. E., Meleux, F., Sciare, J., Crenn, V., and
761 Bonne, J. L.: Role of the boundary layer dynamics effects on an extreme air pollution event in Paris, Atmos.
762 Environ., 141, 571–579, https://doi.org/10.1016/j.atmosenv.2016.06.061, 2016.

763 European Environment Agency, 2023. Harm to human health from air pollution in Europe: burden of disease 2023.
764 https://www.eea.europa.eu/publications/harm-to-human-health-from-air-pollution (accessed 3.4.24).

765 Favez, O., Cachier, H., Sciare, J., and Le Moullec, Y.: Characterization and contribution to PM2.5 of semi-volatile
766 aerosols in Paris (France), Atmos. Environ., 41, 7969–7976, https://doi.org/10.1016/j.atmosenv.2007.09.031,
767 2007.

768 Favez, O., El Haddad, I., Piot, C., Boréave, A., Abidi, E., Marchand, N., Jaffrezo, J.-L., Besombes, J.-L.,
769 Personnaz, M.-B., Sciare, J., Wortham, H., George, C., and D'Anna, B.: Inter-comparison of source apportionment
770 models for the estimation of wood burning aerosols during wintertime in an Alpine city (Grenoble, France),
771 Atmospheric Chem. Phys., 10, 5295–5314, https://doi.org/10.5194/acp-10-5295-2010, 2010.

772 Favez, O., Weber, S., Petit, J.-E., Alleman, L.Y., Albinet, A., Riffault, V., Chazeau, B., Amodeo, T., Salameh, D.,
773 Zhang, Y., Srivastava, D., Samaké, A., Aujay-Plouzeau, R., Papin, A., Bonnaire, N., Boullanger, C., Chatain, M.,
774 Chevrier, F., Detournay, A., Dominik-Sègue, M., Falhun, R., Garbin, C., Ghersi, V., Grignion, G., Levigoureux,
775 G., Pontet, S., Rangognio, J., Zhang, S., Besombes, J.-L., Conil, S., Uzu, G., Savarino, J., Marchand, N., Gros, V.,
776 Marchand, C., Jaffrezo, J.-L., Leoz-Garziandia, E., 2021. Overview of the French Operational Network for In Situ
777 Observation of PM Chemical Composition and Sources in Urban Environments (CARA Program). Atmosphere
778 12, 207. https://doi.org/10.3390/atmos12020207.

779 Flentje, H., Mattis, I., Kipling, Z., Rémy, S., and Thomas, W.: Evaluation of ECMWF IFS-AER (CAMS)
780 operational forecasts during cycle 41r1–46r1 with calibrated ceilometer profiles over Germany, Geosci. Model
781 Dev., 14, 1721–1751, https://doi.org/10.5194/gmd-14-1721-2021, 2021.

782 Foret, G., Michoud, V., Kotthaus, S., Petit, J.-E., Baudic, A., Siour, G., Kim, Y., Doussin, J.-F., Dupont, J.-C.,
783 Formenti, P., Gaimoz, C., Ghersi, V., Gratien, A., Gros, V., Jaffrezo, J.-L., Haeffelin, M., Kreitz, M., Ravetta, F.,

784 Sartelet, K., Simon, L., Té, Y., Uzu, G., Zhang, S., Favez, O., and Beekmann, M.: The December 2016 extreme
785 weather and particulate matter pollution episode in the Paris region (France), Atmos. Environ., 291, 119386,
786 https://doi.org/10.1016/j.atmosenv.2022.119386, 2022.

787 Forster, P.M., Smith, C.J., Walsh, T., Lamb, W.F., Lamboll, R., Hauser, M., Ribes, A., Rosen, D., Gillett, N.,
788 Palmer, M.D., Rogelj, J., von Schuckmann, K., Seneviratne, S.I., Trewin, B., Zhang, X., Allen, M., Andrew, R.,
789 Birt, A., Borger, A., Boyer, T., Broersma, J.A., Cheng, L., Dentener, F., Friedlingstein, P., Gutiérrez, J.M.,
790 Gütschow, J., Hall, B., Ishii, M., Jenkins, S., Lan, X., Lee, J.-Y., Morice, C., Kadow, C., Kennedy, J., Killick, R.,
791 Minx, J.C., Naik, V., Peters, G.P., Pirani, A., Pongratz, J., Schleussner, C.-F., Szopa, S., Thorne, P., Rohde, R.,
792 Rojas Corradi, M., Schumacher, D., Vose, R., Zickfeld, K., Masson-Delmotte, V., Zhai, P., 2023. Indicators of
793 Global Climate Change 2022: annual update of large-scale indicators of the state of the climate system and human
794 influence. Earth System Science Data 15, 2295–2327. https://doi.org/10.5194/essd-15-2295-2023.

795 Fortems-Cheiney, A., Dufour, G., Hamaoui-Laguel, L., Foret, G., Siour, G., Van Damme, M., Meleux, F., Coheur,
796 P.-F., Clerbaux, C., Clarisse, L., Favez, O., Wallasch, M., and Beekmann, M.: Unaccounted variability in NH3
797 agricultural sources detected by IASI contributing to European spring haze episode, Geophys. Res. Lett., 43, 5475–
798 5482, https://doi.org/10.1002/2016GL069361, 2016.

799 Freney, E., Zhang, Y., Croteau, P., Amodeo, T., Williams, L., Truong, F., Petit, J.-E., Sciare, J., Sarda-Esteve, R.,
800 Bonnaire, N., Arumae, T., Aurela, M., Bougiatioti, A., Mihalopoulos, N., Coz, E., Artinano, B., Crenn, V., Elste,
801 T., Heikkinen, L., Poulain, L., Wiedensohler, A., Herrmann, H., Priestman, M., Alastuey, A., Stavroulas, I., Tobler,
802 A., Vasilescu, J., Zanca, N., Canagaratna, M., Carbone, C., Flentje, H., Green, D., Maasikmets, M., Marmureanu,
803 L., Minguillon, M. C., Prevot, A. S. H., Gros, V., Jayne, J., and Favez, O.: The second ACTRIS inter-comparison
804 (2016) for Aerosol Chemical Speciation Monitors (ACSM): Calibration protocols and instrument performance
805 evaluations, Aerosol Sci. Technol., 53, 830–842, https://doi.org/10.1080/02786826.2019.1608901, 2019.

806 Fuzzi, S., Baltensperger, U., Carslaw, K., Decesari, S., Denier van der Gon, H., Facchini, M. C., Fowler, D., Koren,
807 I., Langford, B., Lohmann, U., Nemitz, E., Pandis, S., Riipinen, I., Rudich, Y., Schaap, M., Slowik, J. G.,
808 Spracklen, D. V., Vignati, E., Wild, M., Williams, M., and Gilardoni, S.: Particulate matter, air quality and climate:
809 lessons learned and future needs, Atmospheric Chem. Phys., 15, 8217–8299, https://doi.org/10.5194/acp-15-8217-
810 2015, 2015.

811 Heikkinen, L., Äijälä, M., Daellenbach, K. R., Chen, G., Garmash, O., Aliaga, D., Graeffe, F., Räty, M., Luoma,
812 K., Aalto, P., Kulmala, M., Petäjä, T., Worsnop, D., and Ehn, M.: Eight years of sub-micrometre organic aerosol
813 composition data from the boreal forest characterized using a machine-learning approach, Atmospheric Chem.
814 Phys., 21, 10081–10109, https://doi.org/10.5194/acp-21-10081-2021, 2021.

815 Jacobson, M. Z.: Strong radiative heating due to the mixing state of black carbon in atmospheric aerosols, Nature,
816 409, 695–697, https://doi.org/10.1038/35055518, 2001.

817 Janssen, N. A. H., Hoek, G., Simic, -Lawson Milena, Fischer, P., van, B. L., ten, B. H., Keuken, M., Atkinson, R.
818 W., Anderson, H. R., Brunekreef, B., and Cassee, F. R.: Black Carbon as an Additional Indicator of the Adverse

819 Health Effects of Airborne Particles Compared with PM10 and PM2.5, Environ. Health Perspect., 119, 1691–
820 1699, https://doi.org/10.1289/ehp.1003369, 2011.

821 Kiendler-Scharr, A., Mensah, A.A., Friese, E., Topping, D., Nemitz, E., Prevot, A.S.H., Äijälä, M., Allan, J.,
822 Canonaco, F., Canagaratna, M., Carbone, S., Crippa, M., Dall Osto, M., Day, D.A., De Carlo, P., Di Marco, C.F.,
823 Elbern, H., Eriksson, A., Freney, E., Hao, L., Herrmann, H., Hildebrandt, L., Hillamo, R., Jimenez, J.L.,
824 Laaksonen, A., McFiggans, G., Mohr, C., O'Dowd, C., Otjes, R., Ovadnevaite, J., Pandis, S.N., Poulain, L.,
825 Schlag, P., Sellegri, K., Swietlicki, E., Tiitta, P., Vermeulen, A., Wahner, A., Worsnop, D., Wu, H.-C., 2016.
826 Ubiquity of organic nitrates from nighttime chemistry in the European submicron aerosol. Geophys. Res. Lett. 43,
827 7735–7744. https://doi.org/10.1002/2016GL069239.

828 Kuenen, J., Dellaert, S., Visschedijk, A., Jalkanen, J.-P., Super, I., and Denier van der Gon, H.: CAMS-REG-v4:
829 a state-of-the-art high-resolution European emission inventory for air quality modelling, Earth Syst. Sci. Data, 14,
830 491–515, https://doi.org/10.5194/essd-14-491-2022, 2022.

831 P. Laj, C. L. Myhre, V. Riffault, V. Amiridis, H. Fuchs, K. Eleftheriadis, T. Petäjä, N. Kivekäs, E. Juurola, G.
832 Saponaro, S. Philippin, C. Cornacchia, L. Alados Arboledas, H. Baars, A. Claude, M. De Mazière, B. Dils, L. Eder
833 Murberg, M. Fiebig, M. Haeffelin, H. Herrmann, K. Höhler, N. Illmann, A. Kreuter, E. Ludewig, E. Marinou, O.
834 Möhler, L. Mona, D. Nicolae, E. O'connor, R. M. Petracca Altieri, B. Picquet-Varrault, B. Popsichal, J.-P. Putaud,
835 S. Reimann, T. Salameh, N. Siomos, I. Stachlewska, D. Van Pinxteren, K. A. Voudouri, U. Wandiger, A.
836 Wiedensohler, A. Apituley, A. Comeron, M. Gysel-Beer, N. Mihalopoulos, N. Nikolova, A. Pietruczuk, S.
837 Sauvage, J. Sciare, H. Skov, T. Svendby, E. Swietlicki, D. Tonev, G. Vaughan, V. Zdimal, U. Baltensperger, J.-F.
838 Doussin, M. Kulmala, G. Pappalardo, S. Sorvari Sundet, M. Vana, Aerosol, Cloud and Trace Gases Research
839 Infrastructure - ACTRIS, the European research infrastructure supporting atmospheric science, in revision for
840 Bulletin of the American Meteorological Society.

841 Lanz, V. A., Prévôt, A. S. H., Alfarra, M. R., Weimer, S., Mohr, C., DeCarlo, P. F., Gianini, M. F. D., Hueglin,
842 C., Schneider, J., Favez, O., D'Anna, B., George, C., and Baltensperger, U.: Characterization of aerosol chemical
843 composition with aerosol mass spectrometry in Central Europe: an overview, Atmospheric Chem. Phys., 10,
844 10453–10471, https://doi.org/10.5194/acp-10-10453-2010, 2010.

845 LCSQA: Guide méthodologique pour la mesure du « Black Carbon » par Aethalomètre multi longueur d'onde
846 AE33 dans l'air ambiant (Version 2020), 2020.

847 LCSQA: CAHIER DES CHARGES POUR L'ETALONNAGE DES Q-ACSM, 2022.

848 Liu, P.S.K., Deng, R., Smith, K.A., Williams, L.R., Jayne, J.T., Canagaratna, M.R., Moore, K., Onasch, T.B.,
849 Worsnop, D.R., Deshler, T., 2007. Transmission Efficiency of an Aerodynamic Focusing Lens System:
850 Comparison of Model Calculations and Laboratory Measurements for the Aerodyne Aerosol Mass Spectrometer.
851 Aerosol Science and Technology 41, 721–733. https://doi.org/10.1080/02786820701422278.

852   Menut, L., Bessagnet, B., Briant, R., Cholakian, A., Couvidat, F., Mailler, S., Pennel, R., Siour, G., Tuccella, P.,

853   Turquety, S., and Valari, M.: The CHIMERE v2020r1 online chemistry-transport model, Geosci. Model Dev., 14,

854   6781–6811, https://doi.org/10.5194/gmd-14-6781-2021, 2021.

855   Middlebrook, A. M., Bahreini, R., Jimenez, J. L., and Cana-Garatna, M. R.: Evaluation of Composition-Dependent

856   Collection Efficiencies for the Aerodyne Aerosol Mass Spectrometer using Field Data, Aerosol Sci Technol, 46,

857   258–271, 2011.

858   Nault, B.A., Croteau, P., Jayne, J., Williams, A., Williams, L., Worsnop, D., Katz, E.F., DeCarlo, P.F.,

859   Canagaratna, M., 2023. Laboratory evaluation of organic aerosol relative ionization efficiencies in the aerodyne

860   aerosol mass spectrometer and aerosol chemical speciation monitor. Aerosol Science and Technology 57, 981–

861   997. https://doi.org/10.1080/02786826.2023.2223249.

862   Nenes, A., Pandis, S.N., Pilinis, C., 1998. ISORROPIA: A New Thermodynamic Equilibrium Model for

863   Multiphase   Multicomponent   Inorganic   Aerosols.   Aquatic   Geochemistry   4,   123–152.

864   https://doi.org/10.1023/A:1009604003981.

865   Ng, N. L., Herndon, S. C., Trimborn, A., Canagaratna, M. R., Croteau, P. L., Onasch, T. B., Sueper, D., Worsnop,

866   D. R., Zhang, Q., Sun, Y. L., and Jayne, J. T.: An Aerosol Chemical Speciation Monitor (ACSM) for Routine

867   Monitoring of the Composition and Mass Concentrations of Ambient Aerosol, Aerosol Sci. Technol., 45, 780–

868   794, https://doi.org/10.1080/02786826.2011.560211, 2011a.

869   Ng, N. L., Canagaratna, M. R., Jimenez, J. L., Zhang, Q., Ulbrich, I. M., and Worsnop, D. R.: Real-Time Methods

870   for Estimating Organic Component Mass Concentrations from Aerosol Mass Spectrometer Data, Environ. Sci.

871   Technol., 45, 910–916, https://doi.org/10.1021/es102951k, 2011b.

872   Petit, J.-E., Favez, O., Sciare, J., Crenn, V., Sarda-Estève, R., Bonnaire, N., Močnik, G., Dupont, J.-C., Haeffelin,

873   M., and Leoz-Garziandia, E.: Two years of near real-time chemical composition of submicron aerosols in the

874   region of Paris using an Aerosol Chemical Speciation Monitor (ACSM) and a multi-wavelength Aethalometer,

875   Atmospheric Chem. Phys., 15, 2985–3005, https://doi.org/10.5194/acp-15-2985-2015, 2015.

876   Petit, J.-E., Amodeo, T., Meleux, F., Bessagnet, B., Menut, L., Grenier, D., Pellan, Y., Ockler, A., Rocq, B., Gros,

877   V., Sciare, J., and Favez, O.: Characterising an intense PM pollution episode in March 2015 in France from multi-

878   site approach and near real time data: Climatology, variabilities, geographical origins and model evaluation,

879   Atmos. Environ., 155, 68–84, https://doi.org/10.1016/j.atmosenv.2017.02.012, 2017.

880   Pieber, S.M., El Haddad, I., Slowik, J.G., Canagaratna, M.R., Jayne, J.T., Platt, S.M., Bozzetti, C., Daellenbach,

881   K.R., Fröhlich, R., Vlachou, A., Klein, F., Dommen, J., Miljevic, B., Jiménez, J.L., Worsnop, D.R., Baltensperger,

882   U., Prévôt, A.S.H., 2016. Inorganic Salt Interference on CO2+ in Aerodyne AMS and ACSM Organic Aerosol

883   Composition Studies. Environ. Sci. Technol. 50, 10494–10503. https://doi.org/10.1021/acs.est.6b01035.

884   Poulain, L., Spindler, G., Grüner, A., Tuch, T., Stieger, B., van Pinxteren, D., Petit, J.-E., Favez, O., Herrmann,

885   H., Wiedensohler, A., 2020. Multi-year ACSM measurements at the central European research station Melpitz

886 (Germany) – Part 1: Instrument robustness, quality assurance, and impact of upper size cutoff diameter.
887 Atmospheric Measurement Techniques 13, 4973–4994. https://doi.org/10.5194/amt-13-4973-2020.

888 Putaud, J.-P., Raes, F., Van Dingenen, R., Brüggemann, E., Facchini, M.-C., Decesari, S., Fuzzi, S., Gehrig, R.,
889 Hüglin, C., Laj, P., Lorbeer, G., Maenhaut, W., Mihalopoulos, N., Müller, K., Querol, X., Rodriguez, S., Schneider,
890 J., Spindler, G., Brink, H. ten, Tørseth, K., and Wiedensohler, A.: A European aerosol phenomenology—2:
891 chemical characteristics of particulate matter at kerbside, urban, rural and background sites in Europe, Atmos.
892 Environ., 38, 2579–2595, https://doi.org/10.1016/j.atmosenv.2004.01.041, 2004.

893 Roig Rodelas, R., Perdrix, E., Herbin, B., and Riffault, V.: Characterization and variability of inorganic aerosols
894 and their gaseous precursors at a suburban site in northern France over one year (2015–2016), Atmos. Environ.,
895 200, 142–157, https://doi.org/10.1016/j.atmosenv.2018.11.041, 2019.

896 Roig Rodelas, R., Chakraborty, A., Perdrix, E., Tison, E., Riffault, V., 2019. Real-time assessment of wintertime
897 organic aerosol characteristics and sources at a suburban site in northern France. Atmos. Environ. 203, 48–61.
898 https://doi.org/10.1016/j.atmosenv.2019.01.035.

899 Roldin, P., Ehn, M., Kurtén, T., Olenius, T., Rissanen, M. P., Sarnela, N., Elm, J., Rantala, P., Hao, L., Hyttinen,
900 N., Heikkinen, L., Worsnop, D. R., Pichelstorfer, L., Xavier, C., Clusius, P., Öström, E., Petäjä, T., Kulmala, M.,
901 Vehkamäki, H., Virtanen, A., Riipinen, I., and Boy, M.: The role of highly oxygenated organic molecules in the
902 Boreal aerosol-cloud-climate system, Nat. Commun., 10, 4370, https://doi.org/10.1038/s41467-019-12338-8,
903 2019.

904 Sandradewi, J., Prévôt, A. S. H., Szidat, S., Perron, N., Alfarra, M. R., Lanz, V. A., Weingartner, E., and
905 Baltensperger, U.: Using Aerosol Light Absorption Measurements for the Quantitative Determination of Wood
906 Burning and Traffic Emission Contributions to Particulate Matter, Environ. Sci. Technol., 42, 3316–3323,
907 https://doi.org/10.1021/es702253m, 2008.

908 Sartelet, K., Couvidat, F., Wang, Z., Flageul, C., and Kim, Y.: SSH-Aerosol v1.1: A Modular Box Model to
909 Simulate   the   Evolution   of   Primary   and   Secondary   Aerosols,   Atmosphere,   11,   525,
910 https://doi.org/10.3390/atmos11050525, 2020.

911 Saunders, S. M., Jenkin, M. E., Derwent, R. G., and Pilling, M. J.: Protocol for the development of the Master
912 Chemical Mechanism, MCM v3 (Part A): tropospheric degradation of non-aromatic volatile organic compounds,
913 Atmospheric Chem. Phys., 3, 161–180, https://doi.org/10.5194/acp-3-161-2003, 2003.

914 Savadkoohi, M., Pandolfi, M., Reche, C., Niemi, J. V., Mooibroek, D., Titos, G., Green, D. C., Tremper, A. H.,
915 Hueglin, C., Liakakou, E., Mihalopoulos, N., Stavroulas, I., Artiñano, B., Coz, E., Alados-Arboledas, L., Beddows,
916 D., Riffault, V., De Brito, J. F., Bastian, S., Baudic, A., Colombi, C., Costabile, F., Chazeau, B., Marchand, N.,
917 Gómez-Amo, J. L., Estellés, V., Matos, V., van der Gaag, E., Gille, G., Luoma, K., Manninen, H. E., Norman, M.,
918 Silvergren, S., Petit, J.-E., Putaud, J.-P., Rattigan, O. V., Timonen, H., Tuch, T., Merkel, M., Weinhold, K.,
919 Vratolis, S., Vasilescu, J., Favez, O., Harrison, R. M., Laj, P., Wiedensohler, A., Hopke, P. K., Petäjä, T., Alastuey,

A., and Querol, X.: The variability of mass concentrations and source apportionment analysis of equivalent black carbon across urban Europe, Environ. Int., 178, 108081, https://doi.org/10.1016/j.envint.2023.108081, 2023.

Savadkoohi, M., Pandolfi, M., Favez, O., Putaud, J.-P., Eleftheriadis, K., Fiebig, M., Hopke, P.K., Laj, P., Wiedensohler, A., Alados-Arboledas, L., Bastian, S., Chazeau, B., María, Á.C., Colombi, C., Costabile, F., Green, D.C., Hueglin, C., Liakakou, E., Luoma, K., Listrani, S., Mihalopoulos, N., Marchand, N., Močnik, G., Niemi, J.V., Ondráček, J., Petit, J.-E., Rattigan, O.V., Reche, C., Timonen, H., Titos, G., Tremper, A.H., Vratolis, S., Vodička, P., Funes, E.Y., Zíková, N., Harrison, R.M., Petäjä, T., Alastuey, A., Querol, X., 2024. Recommendations for reporting equivalent black carbon (eBC) mass concentrations based on long-term pan-European in-situ observations. Environment International 185, 108553. https://doi.org/10.1016/j.envint.2024.108553.

Schaap, M., Spindler, G., Schulz, M., Acker, K., Maenhaut, W., Berner, A., Wieprecht, W., Streit, N., Müller, K., Brüggemann, E., Chi, X., Putaud, J.-P., Hitzenberger, R., Puxbaum, H., Baltensperger, U., and ten Brink, H.: Artefacts in the sampling of nitrate studied in the "INTERCOMP" campaigns of EUROTRAC-AEROSOL, Atmos. Environ., 38, 6487–6496, https://doi.org/10.1016/j.atmosenv.2004.08.026, 2004.

Sun, J., Zhang, Q., Canagaratna, M. R., Zhang, Y., Ng, N. L., Sun, Y., Jayne, J. T., Zhang, X., Zhang, X., and Worsnop, D. R.: Highly time- and size-resolved characterization of submicron aerosol particles in Beijing using an Aerodyne Aerosol Mass Spectrometer, Atmos. Environ., 44, 131–140, https://doi.org/10.1016/j.atmosenv.2009.03.020, 2010.

Tobler, A. K., Skiba, A., Wang, D. S., Croteau, P., Styszko, K., Nęcki, J., Baltensperger, U., Slowik, J. G., and Prévôt, A. S. H.: Improved chloride quantification in quadrupole aerosol chemical speciation monitors (Q-ACSMs), Atmospheric Meas. Tech., 13, 5293–5301, https://doi.org/10.5194/amt-13-5293-2020, 2020.

Tobler, A. K., Skiba, A., Canonaco, F., Močnik, G., Rai, P., Chen, G., Bartyzel, J., Zimnoch, M., Styszko, K., Nęcki, J., Furger, M., Różański, K., Baltensperger, U., Slowik, J. G., and Prevot, A. S. H.: Characterization of non-refractory (NR) PM_1 and source apportionment of organic aerosol in Kraków, Poland, Atmospheric Chem. Phys., 21, 14893–14906, https://doi.org/10.5194/acp-21-14893-2021, 2021.

Viana, M., Kuhlbusch, T. A. J., Querol, X., Alastuey, A., Harrison, R. M., Hopke, P. K., Winiwarter, W., Vallius, M., Szidat, S., Prévôt, A. S. H., Hueglin, C., Bloemen, H., Wåhlin, P., Vecchi, R., Miranda, A. I., Kasper-Giebl, A., Maenhaut, W., and Hitzenberger, R.: Source apportionment of particulate matter in Europe: A review of methods and results, J. Aerosol Sci., 39, 827–849, https://doi.org/10.1016/j.jaerosci.2008.05.007, 2008.

Wang, Z., Couvidat, F., and Sartelet, K.: GENerator of reduced Organic Aerosol mechanism (GENOA v1.0): an automatic generation tool of semi-explicit mechanisms, Geosci. Model Dev., 15, 8957–8982, https://doi.org/10.5194/gmd-15-8957-2022, 2022.

Wang, Z., Couvidat, F., and Sartelet, K.: Implementation of a parallel reduction algorithm in the GENerator of reduced Organic Aerosol mechanisms (GENOA v2.0): Application to multiple monoterpene aerosol precursors, J. Aerosol Sci., 174, 106248, https://doi.org/10.1016/j.jaerosci.2023.106248, 2023.

954 Wang, Z., Couvidat, F., & Sartelet, K. (2024). Response of biogenic secondary organic aerosol formation to
955 anthropogenic NOx emission mitigation. Science of the Total Environment, 927, 172142.
956 https://doi.org/10.1016/j.scitotenv.2024.172142.

957 Watson, T. B.: Aerosol Chemical Speciation Monitor (ACSM) Instrument Handbook,
958 https://doi.org/10.2172/1375336, 2017.

959 Wittmaack, K. and Keck, L.: Thermodesorption of aerosol matter on multiple filters of different materials for a
960 more detailed evaluation of sampling artifacts, Atmos. Environ., 38, 5205–5215,
961 https://doi.org/10.1016/j.atmosenv.2004.05.047, 2004.

962 WHO Air Quality Guidelines: https://www.c40knowledgehub.org/s/article/WHO-Air-Quality-
963 Guidelines?language=en_US, last access: 23 January 2023.

964 Xu, W., Lambe, A., Silva, P., Hu, W., Onasch, T., Williams, L., Croteau, P., Zhang, X., Renbaum-Wolff, L.,
965 Fortner, E., Jimenez, J.L., Jayne, J., Worsnop, D., Canagaratna, M., 2018. Laboratory evaluation of species-
966 dependent relative ionization efficiencies in the Aerodyne Aerosol Mass Spectrometer. Aerosol Science and
967 Technology 52, 626–641. https://doi.org/10.1080/02786826.2018.1439570.

968 Zanatta, M., Gysel, M., Bukowiecki, N., Müller, T., Weingartner, E., Areskoug, H., Fiebig, M., Yttri, K. E.,
969 Mihalopoulos, N., Kouvarakis, G., Beddows, D., Harrison, R. M., Cavalli, F., Putaud, J. P., Spindler, G.,
970 Wiedensohler, A., Alastuey, A., Pandolfi, M., Sellegri, K., Swietlicki, E., Jaffrezo, J. L., Baltensperger, U., and
971 Laj, P.: A European aerosol phenomenology-5: Climatology of black carbon optical properties at 9 regional
972 background sites across Europe, Atmos. Environ., 145, 346–364, https://doi.org/10.1016/j.atmosenv.2016.09.035,
973 2016.

974 Zhang, S., Tison, E., Dusanter, S., Beaugard, C., Gengembre, C., Augustin, P., Fourmentin, M., Delbarre, H.,
975 Riffault, V., 2021. Near real-time PM1 chemical composition measurements at a French urban background and
976 coastal site under industrial influence over more than a year: Temporal variability and assessment of sulfur-
977 containing emissions. Atmos. Environ. 244, 117960. https://doi.org/10.1016/j.atmosenv.2020.117960.

978 Zhang, Y., Favez, O., Albinet, A., Canonaco, F., Truong, F., Amodeo, T., Prevot, A., Sciare, J., and Gros, V.:
979 Long-term measurements of the chemistry and sources of submicron aerosols at SIRTA in Paris area, France, in:
980 European Aerosol Conference (EAC 2017), Zurich, Switzerland, 2017.

981 Zhang, Y., Favez, O., Petit, J.-E., Canonaco, F., Truong, F., Bonnaire, N., Crenn, V., Amodeo, T., Prévôt, A. S.
982 H., Sciare, J., Gros, V., and Albinet, A.: Six-year source apportionment of submicron organic aerosols from near-
983 continuous highly time-resolved measurements at SIRTA (Paris area, France), Atmospheric Chem. Phys., 19,
984 14755–14776, https://doi.org/10.5194/acp-19-14755-2019, 2019.